CoA Note No.70

CONFIDENTIAL

THE COLLEGE OF AERONAUTICS

CRANFIELD

POST NUBES LUX

THE EFFECT OF JET DEFLECTION ON THE INTERFERENCE OF A REARWARD FACING JET

by

A. H. CRAVEN

M. of S. Contract 7/GEN/1473/PR3

CONFIDENTIAL

NOTE NO. 70
OCTOBER, 1957

THE COLLEGE OF AERONAUTICS

CRANFIELD

The effect of jet deflection on the interference of a rearward facing jet with the flow over an afterbody in a uniform subsonic flow.

by

A. H. Craven, M.Sc., Ph.D., D.C.Ae.

SUMMARY

This paper contains the results of an experimental investigation into the effects induced by a deflected jet upon the body from which it issues. The tests were performed at a Reynolds number of 0.3×10^6 based on body diameter and maximum tunnel velocity.

It was found that a side force and moment were induced upon the afterbody, the magnitude of which increased with jet deflection and jet thrust. The direction of the induced side force was in a direction opposite to the normal component of the thrust vector. The base drag increased with jet thrust but decreased with increase of jet deflection for small deflections.

Prepared under Ministry of Supply Contract 7/GEN/1473/PR3

CONTENTS

List of Symbols

1. Introduction

2. Apparatus

   2.1. The wind tunnel and instruments

   2.2. The models

3. Scope of Tests

4. Test Procedure

5. Results

   5.1. Presentation of Results

   5.2. The pressure distributions

      5.2.1. The base pressures

      5.2.2. Side pressures

   5.3. The forces and moments

      5.3.1. Drag

      5.3.2. Side Force

      5.3.3. Pitching moments

6. Discussion

   6.1. Accuracy of results

   6.2. The flow patterns

   6.3. Dependence on $C_J^{\frac{1}{2}}$

   6.4. Application of the results

7. Conclusions

8. References

Figures

LIST OF SYMBOLS

C_D base drag coefficient in terms of total base area.

C_J jet thrust coefficient $\left(= \dfrac{mv_b}{\frac{1}{2}\rho U_o^2 S} \right)$

C_M total pitching moment coefficient in terms of total base area.

C_{M_B} pitching moment coefficient due to base pressures.

C_{M_N} pitching moment coefficient due to side pressures.

C_N side force coefficient in terms of total base area.

C_p pressure coefficient $\left(= \dfrac{p - p_o}{\frac{1}{2}\rho U_o^2} \right)$

d body diameter

m jet mass flow

p static pressure (suffix o denotes free stream value)

r radial distance from jet centre

R radius of body

S base area $(= \Pi R^2)$

U_o free stream speed

V_b equivalent jet velocity i.e. the velocity attained in an isentropic expansion from jet stagnation pressure to free stream static pressure.

x distance from jet exit in upstream direction.

δ jet deflection angle

θ meridian angle

ρ free stream air density.

see figure 1.

1. Introduction

A previous paper (1) has given the results of experiments to determine the effect of the undeflected jet upon the pressure distribution around three representative afterbodies in a uniform subsonic stream and the effect of the afterbody shape on the drag of the body. The use of the jet is not restricted solely to propulsion; its use, when deflected, as a control has been postulated. The reaction of a deflected jet will produce considerable side forces and moment upon the body from which it issues and these will exist at whatever altitude the jet is operating and depend only on the jet thrust and deflection angle. However the deflected jet also interferes asymmetrically with the flow around the afterbody and thereby produces side forces and moments which will affect the control capabilities of the deflected jet. Furthermore the changes in base pressure due to jet deflection will result in changes in the form drag.

Theoretical papers by Spence (2) and Stratford (3) and experimental investigations by Dimmock (4), Davidson (5) and others have explored the analogous two-dimensional problem. Although no theoretical solution of the problems of a circular body with deflected jet has been published to the knowledge of the author, yet an approximate application of slender body theory leads to the conclusion that, in inviscid flow, the lateral force on the body will be zero. It is therefore the purpose of the present paper to ascertain how the viscous effects, including the areas of separation, modify this result. To this end experiments were conducted to investigate these induced effects and in particular to determine the pressure distributions on the base and side surfaces of a bluff cylindrical afterbody from which a deflected jet issues. From these the side force, base drag and pitching moment induced on the afterbody by the interference of the jet with the subsonic free stream are calculated.

The experiments described herein are the second phase of a fuller investigation into the effect of jet flow sponsored by the Ministry of Supply under Contract No. 7/Gen/1473/PR3. The author would like to thank Mr. S. H. Lilley for the design and erection of the equipment, Mr. H. Stanton for the care and enthusiasm with which he made the models, Mr. Brian Hayden who, with other laboratory assistants, was responsible for taking the experimental measurements, and Mr. F.M. Burrows for preparing Figure 13.

2. Apparatus

2.1. The wind tunnel and instrumentation

The tests were performed in a straight-through wind tunnel having a closed working section measuring 3 ft. square. The installation of the models and the instrumentation have been described in ref.1.

2.2. The models

The external shape of each model was the same; a light alloy cylinder 12" long and 4" in diameter. Polythene pressure tubes for pressure measurements were let into slots along the model's generators and the base radii at angular intervals of $22\frac{1}{2}^{\circ}$. The internal cavity of each model was machined to give a smooth flow into a parallel-sided jet $\frac{3}{4}$" in diameter issuing from the centre of the base of the afterbody at the required angle of deflection. The jet deflection angles used were 2, 5, 10 and 20 degrees. It was found impossible to achieve smooth and uniform flow in the jet with larger deflection within the available diameter of the afterbody.

3. The Scope of the Tests

The tests on each of the models covered a range of free stream speeds from 0 to 120 ft/sec., and a range of "equivalent" jet speeds from 0 to 1500 ft/sec. The equivalent jet speed is that calculated from the jet blowing pressure assuming isentropic expansion to free stream pressure.

In terms of the jet thrust coefficient the range covered was

$$0 \leq C_J \leq 40$$

The Reynolds number based on body diameter and free stream speed of 120 ft/sec was 0.3×10^6.

4. Test Procedure

The ordinary pressure plotting techniques were used in these tests. The details are given in ref. 1.

5. Results

5.1. Presentation of Results

As in the previous work the pressure coefficients and forces and moments were found to be presentable in terms of the non-dimensional thrust coefficient C_J. The jet and free stream velocities are, thereby, not explicitly used.

The pressure distributions are given in tables 1 - 5 and in the form of isobar patterns as follows :-

Fig. 2 (a) Base pressure distribution at zero jet deflection ($\delta = 0^\circ$) for $C_J = 0, 2, 4, 10, 20, 40$.

(b)	Base pressure distribution	$\delta = 10^\circ$ and 20°	$C_J = 2$
(c)	Base pressure distribution	$\delta = 10^\circ$ and 20°	$C_J = 4$
(d)	Base pressure distribution	$\delta = 10^\circ$ and 20°	$C_J = 10$
(e)	Base pressure distribution	$\delta = 10^\circ$ and 20°	$C_J = 20$
(f)	Base pressure distribution	$\delta = 10^\circ$ and 20°	$C_J = 40$

Fig. 5 (a) Side pressure distribution (not in isobar form) plotted against x/d for $C_J = 0, 2, 4, 10, 20, 40$.

(b)	Side pressure distribution	$\delta = 10^\circ$ and 20°	$C_J = 2$
(c)	Side pressure distribution	$\delta = 10^\circ$ and 20°	$C_J = .4$
(d)	Side pressure distribution	$\delta = 10^\circ$ and 20°	$C_J = 10$
(e)	Side pressure distribution	$\delta = 10^\circ$ and 20°	$C_J = 20$
(f)	Side pressure distribution	$\delta = 10^\circ$ and 20°	$C_J = 40$

In interpreting fig. 2 the jet is to be regarded as emerging from the plane of the paper and deflected by the appropriate angle towards the bottom of the page. The isobar pattern is thus symmetrical about the plane of the jet and the body centre line and hence the distributions for jet deflections of 10° and 20° are placed side by side for easy comparison. The origin for the meridian angle θ is in the lower plane of symmetry.

In fig. 5 the isobars are plotted on axes of non-dimensional distance ($^x/d$) upstream of the base and meridian angle θ.

Typical radial pressure distributions are given in figs. 3 and 4. Fig. 3 shows the dependence of the pressure coefficient upon jet deflection and fig. 4 gives the variation with meridian angle; both figures being plotted for fixed values of C_J.

By integrating the appropriate pressure distributions the coefficients of base drag, normal force, pitching moment due to base pressure variations, pitching moment due to side pressure variations and total pitching moment have been calculated and are given in figs. 6 - 10 respectively plotted against C_J for given values of θ and against θ for particular values of C_J.

In all the curves drawn the jet has not reached the overchoked condition.

5.2. The Pressure Distributions

5.2.1. The base pressures (figs. 2A - F)

The general trend of the pressure distribution on the base remains unaltered as the jet is deflected. The base suction increases with radius to a peak at approximately $\frac{r}{R} = .8$ and then decreases (figs. 3 and 4). For any particular value of C_J and $\frac{r}{R}$, the variation of pressure coefficient with meridian angle shows an increase in suction from $\theta = 0^\circ$ to 45° and then a decrease to $\theta = 180^\circ$ (fig. 2). In other words the maximum suction does not occur immediately beneath the deflected jet but at nearly 45° from the plane of the jet. Furthermore the position of the peak suction moves outwards as the jet deflection angle increases for values of the meridian angle θ less than 45° (fig.3),

e.g.

$$\frac{r}{R} = .7 \text{ for } \delta = 0^\circ$$

$$\frac{r}{R} = .74 \text{ for } \delta = 10^\circ$$

$$\frac{r}{R} = .8 \text{ for } \delta = 20^\circ$$

when $\theta = 0^\circ$

whereas at larger value of Θ the radial position of the peak suction is sensibly independent of the jet deflection angle.

At zero jet deflection and at about $\frac{r}{R}$ = .6 for all value of C_J there appeared a drop in suction followed immediately by recovery to the peak suction mentioned previously. This same effect is noted with the jet deflected but in modified form. For 2° and 5° deflection the fall in suction is present at approximately $\frac{r}{R}$ = .62 (see fig. 3) throughout the C_J range for all values of meridian angle. For 10° jet deflection the position of this fall in suction has moved to $\frac{r}{R}$ = .68 when $\Theta = 0$ for all values of C_J. As the meridian angle increases the effect is apparent only at successively lower values of C_J and the radial position, where the fall occurs, moves outwards as C_J increases (see fig. 4). The fall in suction has vanished at $\Theta = 180^\circ$. There is no sign of this effect at any value of C_J when the jet deflection angle is 20°.

Depending upon the free stream speed used the jet choked at a particular value of C_J. Any increase of C_J above this value caused a rapid decrease of suction over the base by about ten per cent of its value when the jet choked. The values of the pressure coefficient remained constant if C_J was further increased. The effect was the same for all jet deflections (Table 5). This feature has been omitted from the isobar patterns to avoid confusion.

5.2.2. <u>The side pressure distribution</u> (figs. 5A - F)

As on the base, the presence of the jet increases the slight suction on the side of the body but the effect is negligible at distances greater than two body diameters upstream of the jet exit. For any value of C_J and any value of $^x/d$ the pressure remains approximately constant as the meridian angle Θ increases from 0 to 45°. Further increase of Θ is accompanied by a reduction in suction. Fig. 5 shows that the sharpness of this reduction is directly dependent upon but not proportional to the jet deflection angle.

Except at points very close to the base ($\frac{x}{d} < .05$) the side pressure distribution for the overchoked jet coincided with that for the choked jet case at the same angle of deflection and tunnel speed.

5.3. The Forces and Moments

The force and moment coefficients are obtained by dividing the particular force by $\frac{1}{2}\rho U_o^2 S$, S being the base area of the afterbody, and the moment by $\frac{1}{2}\rho U_o^2 Sd$ where d is the base diameter. The origin for moments is the centre of the base.

5.3.1. Base Drag (fig. 6)

The base drag coefficient increases with increase of C_J for all values of jet deflection angle. The increase is large initially but moderates as C_J increases.

A second important feature is that, for any C_J value within the range of these experiments, the drag decreased as the deflection increased up to $\delta = 10^o$, thereafter increasing slightly with δ.

The effect of overchoking the jet on the drag was shown in ref. 1. This effect is repeated at all values of jet deflection within the range $0 \leqslant \delta \leqslant 20^o$.

5.3.2. Side force (fig. 7)

The variation of the pressure with meridian angle on the curved surface of the cylinder produces a resultant side force acting normal to the cylinder in the plane of the jet and body centreline. The magnitude of the sideforce increases sharply with the thrust parameter for small values of C_J. The slope lessens as C_J increases further and, for $C_J > 30$, the sideforce coefficient becomes sensibly constant particularly for small values of the jet deflection. Eor small values of C_J it appears that the maximum induced sideforce has been reached when $\delta = 20^o$. For higher values of C_J however the maximum would appear to occur at higher jet deflection angles.

It should be noted that this sideforce acts normal to the body in the plane of the jet and the centre line of the body so that it tends to reduce the sideforce produced by the component of the jet thrust normal to the body axis.

5.3.3. The pitching moments (figs. 8 - 10)

The pitching moment due to the pressure variation on the base increases with the jet deflection and with increase of the thrust parameter C_J (fig. 8). This is also true of the pitching moment due to the variation of pressure on the curved surfaces (fig. 9) but to a lesser extent. The side pressures produce an effect which is about half the moment derived from the base under similar conditions. It must be noted that the origin has been chosen at the centre of the base and about this point the two moments reinforce each other to give a total moment in the nose down sense (if the jet is deflected downwards). Taken about any other origin the relative magnitudes and signs of the moments would in general be different.

6. Discussion

6.1. Accuracy of results

The jet supply pressure during any one test was maintained at the required value within limits of 2.5 per cent. The tunnel speed could be kept constant to within 1% and the surface pressures measured to 0.02 in. of alcohol. The overall error in the pressure coefficients is therefore expected to be less than 5%.

6.2. The flow pattern

It is found that deflecting the jet causes major modification of the toroidal vortices postulated in the undeflected case (ref.1). Except in the plane of the jet the flow on the base is no longer radial but curves from an attachment line at $\frac{r}{R} = .3$ approximately to a separation line at $\frac{r}{R} = .85$ approximately (see figs. 11 and 12). There is also an indication that there is a weak flow into this separation line inwards from the edge of the base ($\frac{r}{R} = 1$). Such detail is shown in fig. 11 which is typical of the many surface flow pictures taken. Fig. 12 is drawn from fig. 11 with the important features emphasized. Fig. 11 is not detailed enough to deduce precisely what flow exists between the jet exit ($\frac{r}{R} = \frac{3}{16}$) and $\frac{r}{R} = .3$, but other flow pictures suggest that the fluid entrained into the jet at the exit curls into the jet from the attachment line. The separation and attachment lines show little evidence of asymmetry except in strength and vary little in position as C_J changes or with variation of the jet deflection angle. This is consistent with the form and extent of the radial pressure distribution.

The presence of the separation line is to be expected in view of the adverse pressure gradient outboard of the peak suction at $\frac{r}{R} = .8$ approximately and the attachment is confirmed by the minimum suction that occurs at $\frac{r}{R} = .3$ approximately. This can be seen more clearly if the pressure coefficient is plotted against radial distance for any value of meridian angle (e.g. figs. 3 and 4). When the meridian angle approaches 180° there is relatively little variation in the pressure coefficient with radial position. The flow patterns near $\theta = 180^\circ$ show little accretion of fluid and the attachment line is not visible. The separation is strongest at $\theta = 45^\circ$ as confirmed by the high suction lobes there in the isobar patterns. The side boundary layers which separate from the base appear to roll up and form a pair of spiral vortex sheets with origin at the top centre line and which in turn separate from the base at about 45° from the bottom centre line. These vortex sheets pass downstream and are entrained into the jet. From yawmeter traverses in the wake it appears that this vorticity follows the path of the jet and is completely absorbed into the jet in about five body diameters from the jet exit causing the jet cross-section to assume a lemniscate shape (fig. 13).

It will be seen (from figs. 11 and 12) that there are no features in the surface flow patterns which correspond to the first suction peak at $\frac{r}{R} = 0.6$ (figs. 3 and 4). The form of the pressure distribution however is consistent with the development of a laminar type boundary layer up to $\frac{r}{R} = 0.6$ followed by laminar separation and turbulent reattachment. Turbulent separation then occurs, as stated above, at $\frac{r}{R} = 0.8$ approximately. It can only be assumed that the liquid film has changed the character of the flow in this region.

None of the usual flow visualisation techniques proved satisfactory as the magnitude of the shear velocities involved vary enormously over the base and the pattern produced by one part of the flow was swept clean of detail before that due to another part had developed sufficiently. Furthermore, in these studies, the base of the after-body was vertical and the effect of gravity has also to be taken into account in interpreting the flow patterns. The features of the flow that have been dicussed in this section are definitely shown by the flow patterns but more careful studies may show further detail not apparent in the pictures available at present.

6.3. The dependence on $C_J^{\frac{1}{2}}$

Previous theoretical (2,3) and experimental (4) work on the two-dimensional jet flap has suggested that any induced forces and moments are proportional to $C_J^{\frac{1}{2}}$. Surprisingly enough, if any of the curves of figs. 6 - 10 are plotted against $C_J^{\frac{1}{2}}$ (e.g. fig. 14) it can be seen that the graph is composed of two straight lines, the slope changing abruptly at $C_J = 12$ approximately, this value being independent of the jet deflection angle. There is also a suggestion that there is another change of slope at $C_J = 30$ approximately. Only three points for $C_J \geq 30$ are available and none for $C_J > 40$; the quantity of compressed air available being insufficient to extend the programme further.

The reason for these discontinuities in slope is not clear. It is unlikely to be due to the reduction in tunnel speed necessary to obtain the high values of C_J since the points obtained from experiments at one speed overlap, and merge smoothly with, points obtained at other speeds. The only other explanation lies in some change in the vortex pattern on the base which occurs at the particular values of C_J but which is independent of jet deflection angle. Such changes however do not show on the base flow patterns that have been obtained.

6.4. Application of the results

If the jet is so deflected that its thrust line acts through the centre of gravity of the missile then there is no moment due to the jet reaction. The moment induced by jet interference, which is discussed in this paper, will still remain.

7. Conclusions

(i) Deflection of the jet induces a side force and moment on the bluff afterbody.

(ii) The side force coefficient increases with jet thrust coefficient and jet deflection angle reaching a value of .10 based on base area for $\delta = 20^\circ$ at $C_J = 40$.

(iii) The moment coefficient taken about the centre of the base consists of a moment from the base pressures and one from the side forces. All three increase with jet thrust coefficient and jet deflection angle.

(iv) For given C_J, the base drag decreases as jet deflection increases for $\delta < 10^\circ$. For $\delta > 10^\circ$ the drag increases slightly. For any deflection angle, the base drag increases with C_J.

(v) The induced effects are small compared with the side force and moment produced by the component of the jet reaction resolved normal to the body axis but of sufficient magnitude to be taken into account when assessing the effect of the deflected jet as a form of control.

8. References

1. Craven, A.H. The interference of a rearward facing jet on the flow over three representative afterbody shapes in a uniform subsonic flow. College of Aeronautics Note No. 60, April, 1957.

2. Spence, D.A. Treatment of the jet flap by thin aerofoil theory. R.A.E. report Aero. 2568, November, 1955.

3. Stratford, B.S. Mixing and the jet flap. Aero. Quarterly, Vol.7, August, 1956.

4. Dimmock, N.A. An experimental introduction to the jet flap. N.G.T.E. Rep. R.175, and Some further jet flap experiments. N.G.T.E. Memo M.255.

5. Davidson, I. The Jet Flap. Journal of the Royal Aeronautical Society, J.R.Ae.S. January 1956.

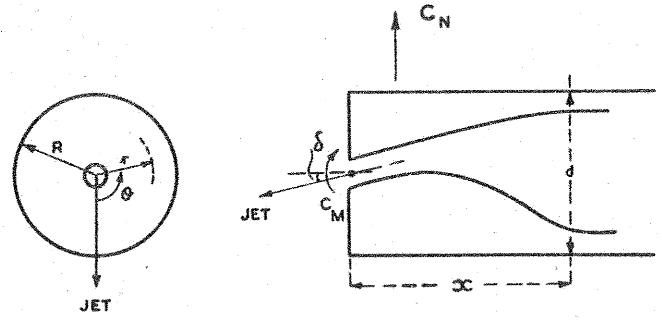

FIG. I. DEFINITION OF SYMBOLS

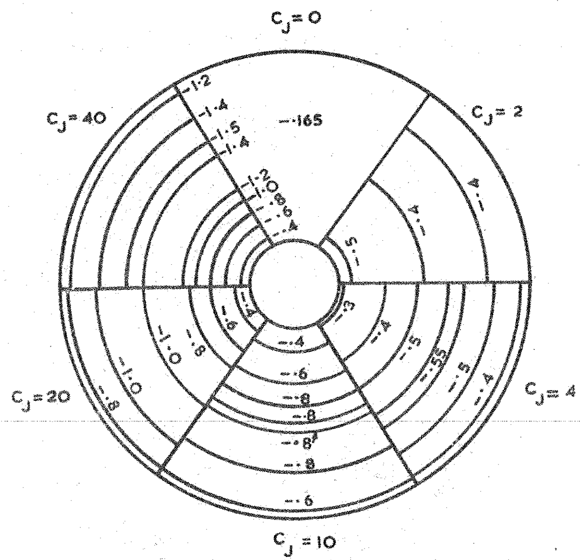

FIG. 2a. PRESSURE DISTRIBUTION ON BASE
ZERO JET DEFLECTION

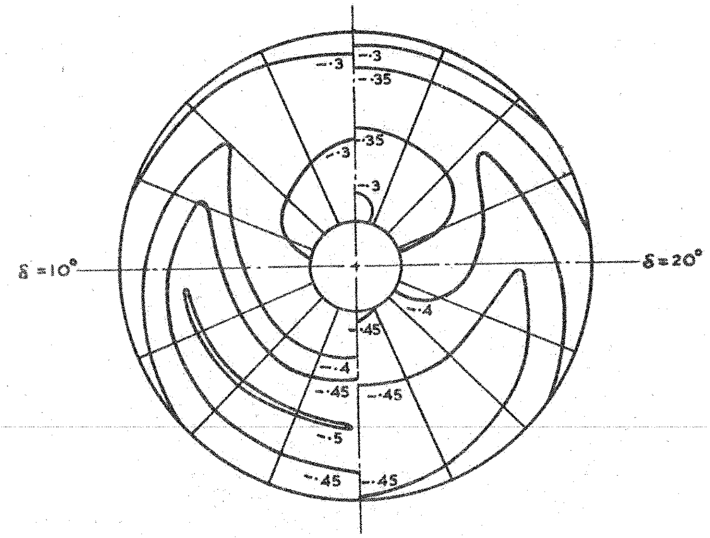

FIG. 2b. BASE PRESSURE DISTRIBUTION C_J = 2

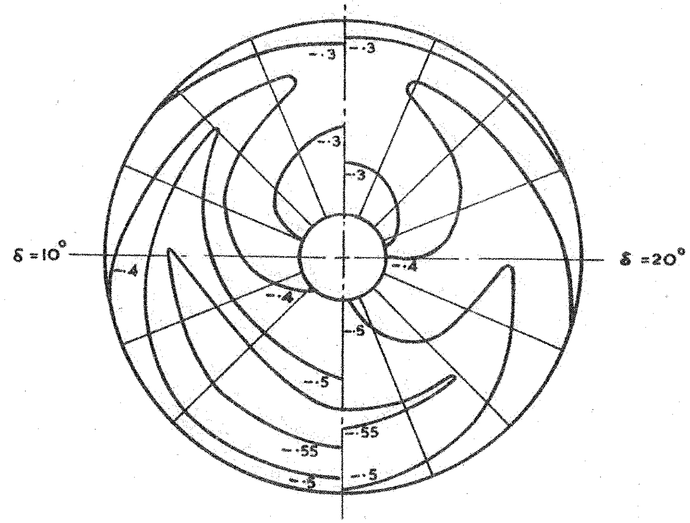

FIG. 2c. BASE PRESSURE DISTRIBUTION $C_J = 4$

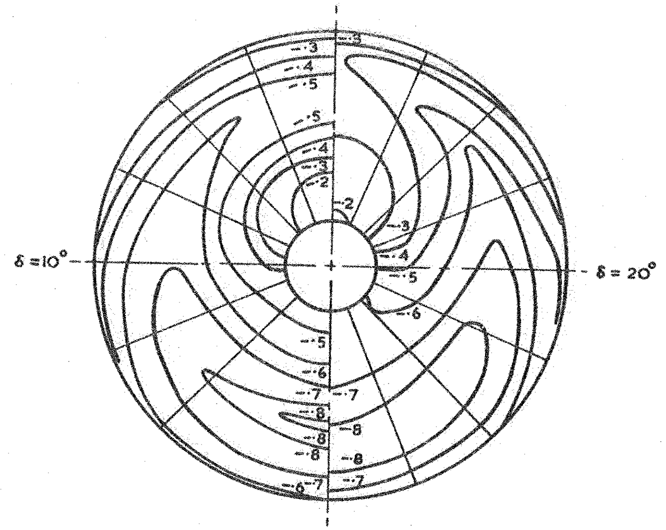

FIG. 2d. BASE PRESSURE DISTRIBUTION $C_J = 10$

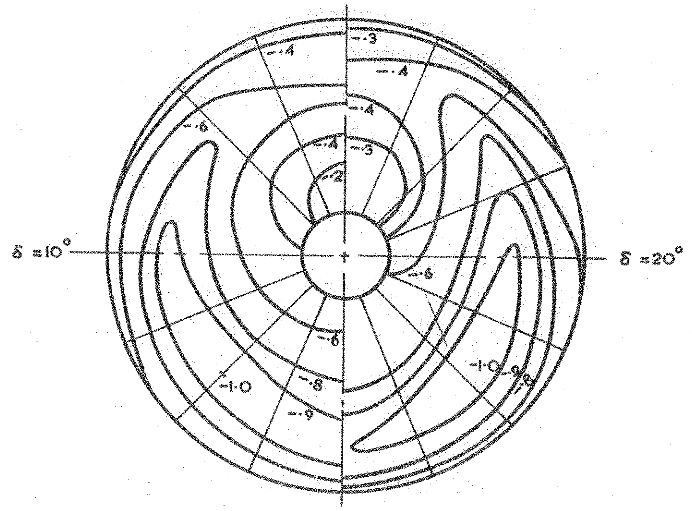

FIG. 2e. BASE PRESSURE DISTRIBUTION $C_J = 20$

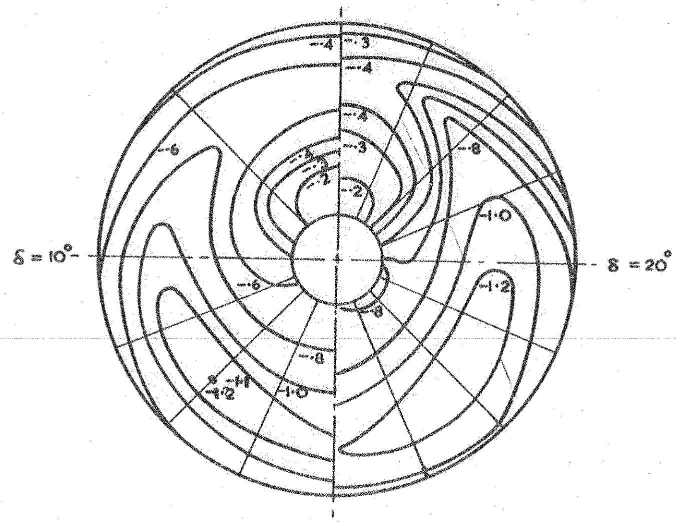

FIG. 2f BASE PRESSURE DISTRIBUTION $C_J = 40$

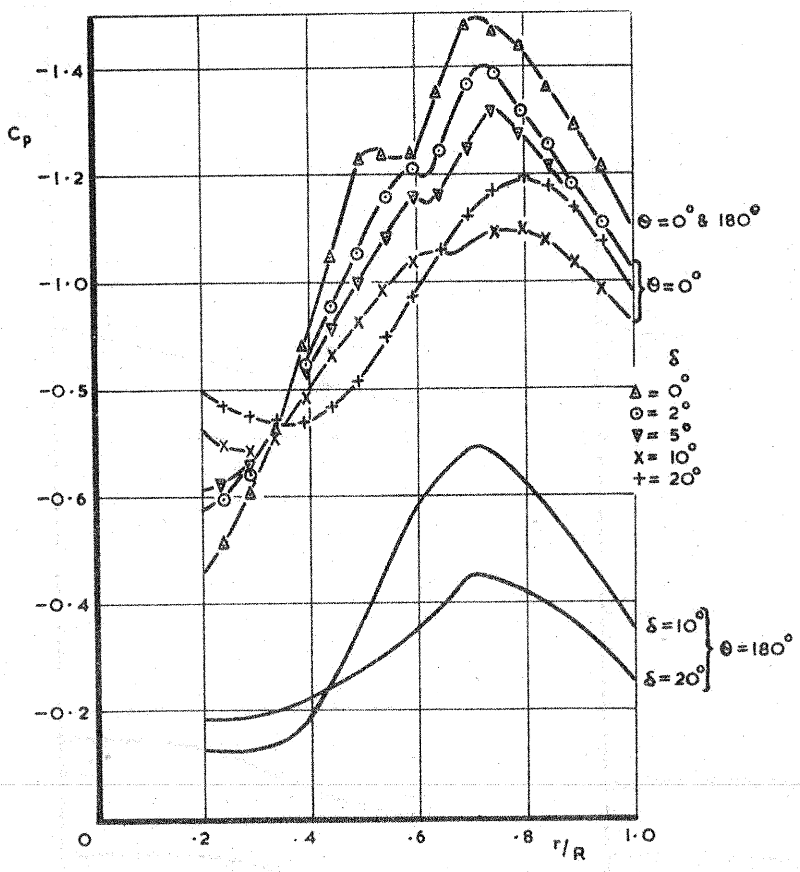

FIG. 3. TYPICAL VARIATION OF RADIAL PRESSURE DISTRIBUTION WITH JET DEFLECTION $C_J = 40$

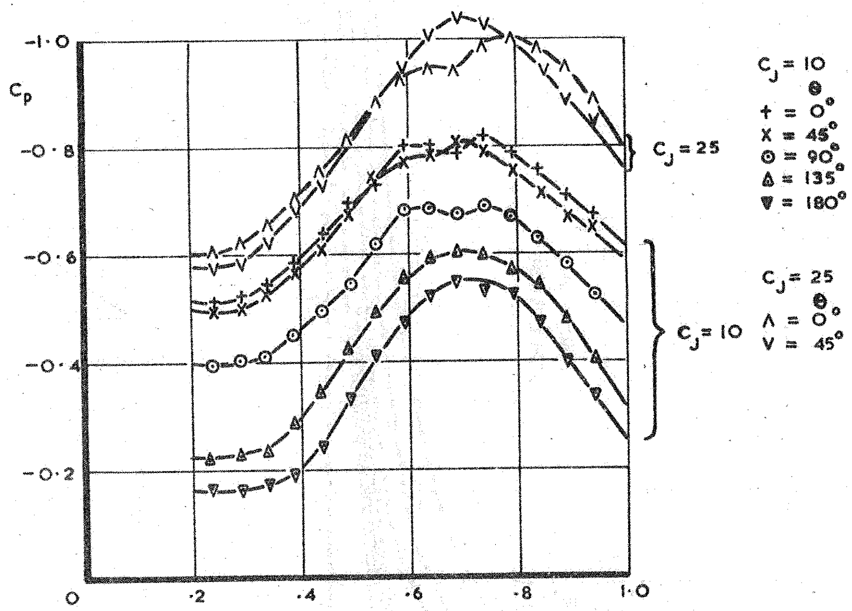

FIG. 4. TYPICAL VARIATION OF RADIAL PRESSURE DISTRIBUTION WITH MERIDIAN ANGLE; JET DEFLECTION θ = 10°

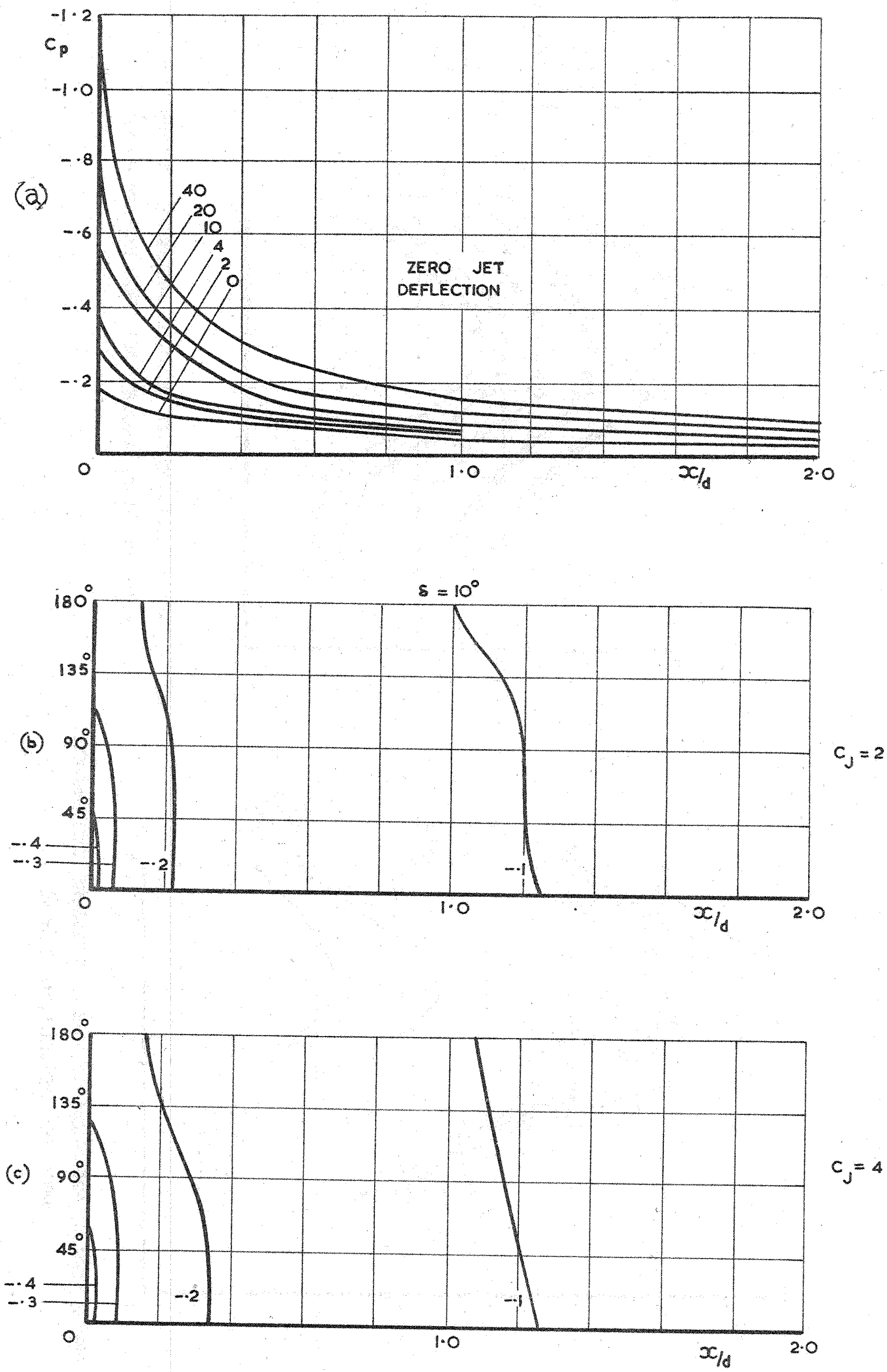

FIG. 5. SIDE PRESSURE DISTRIBUTIONS

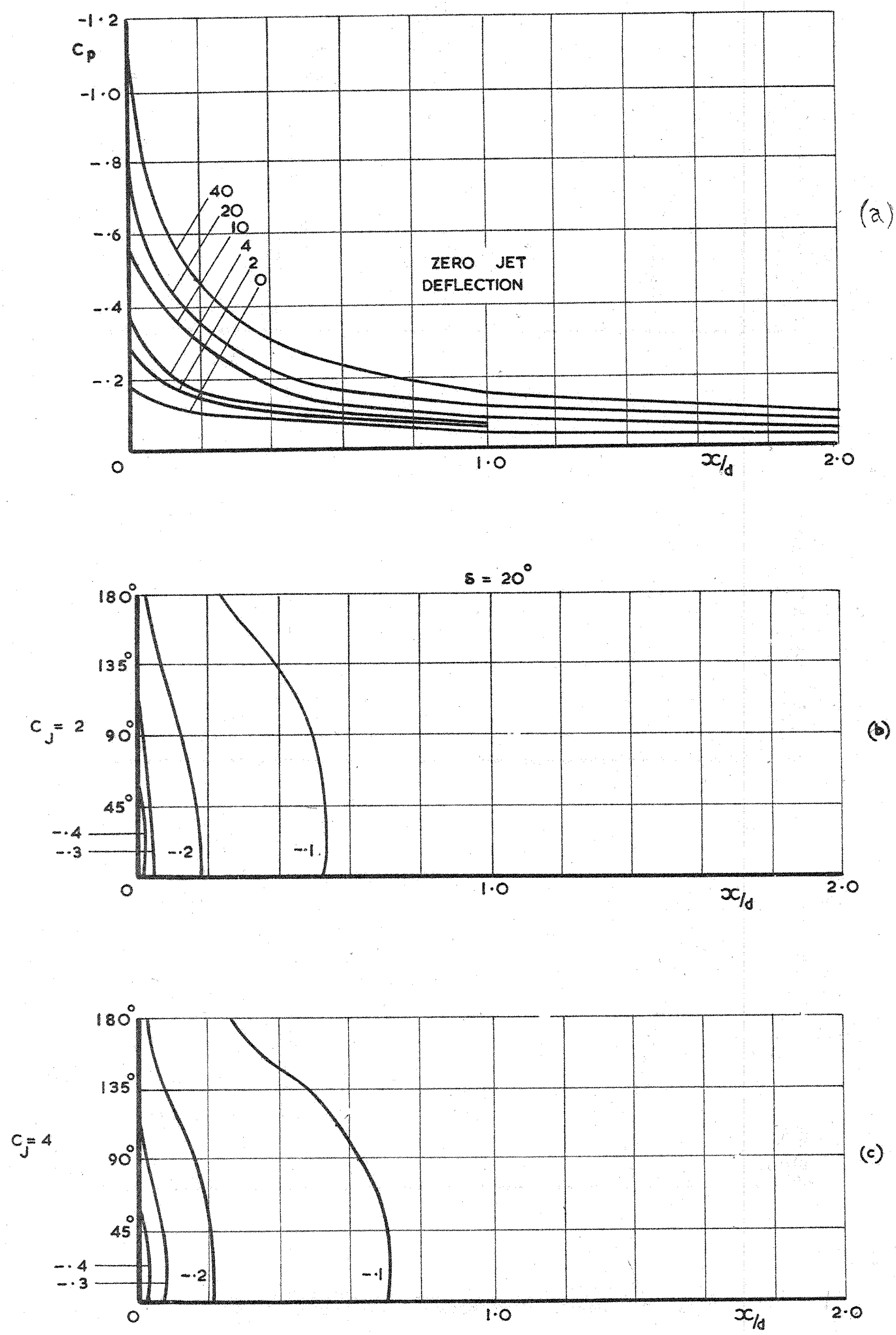

FIG. 5. SIDE PRESSURE DISTRIBUTIONS

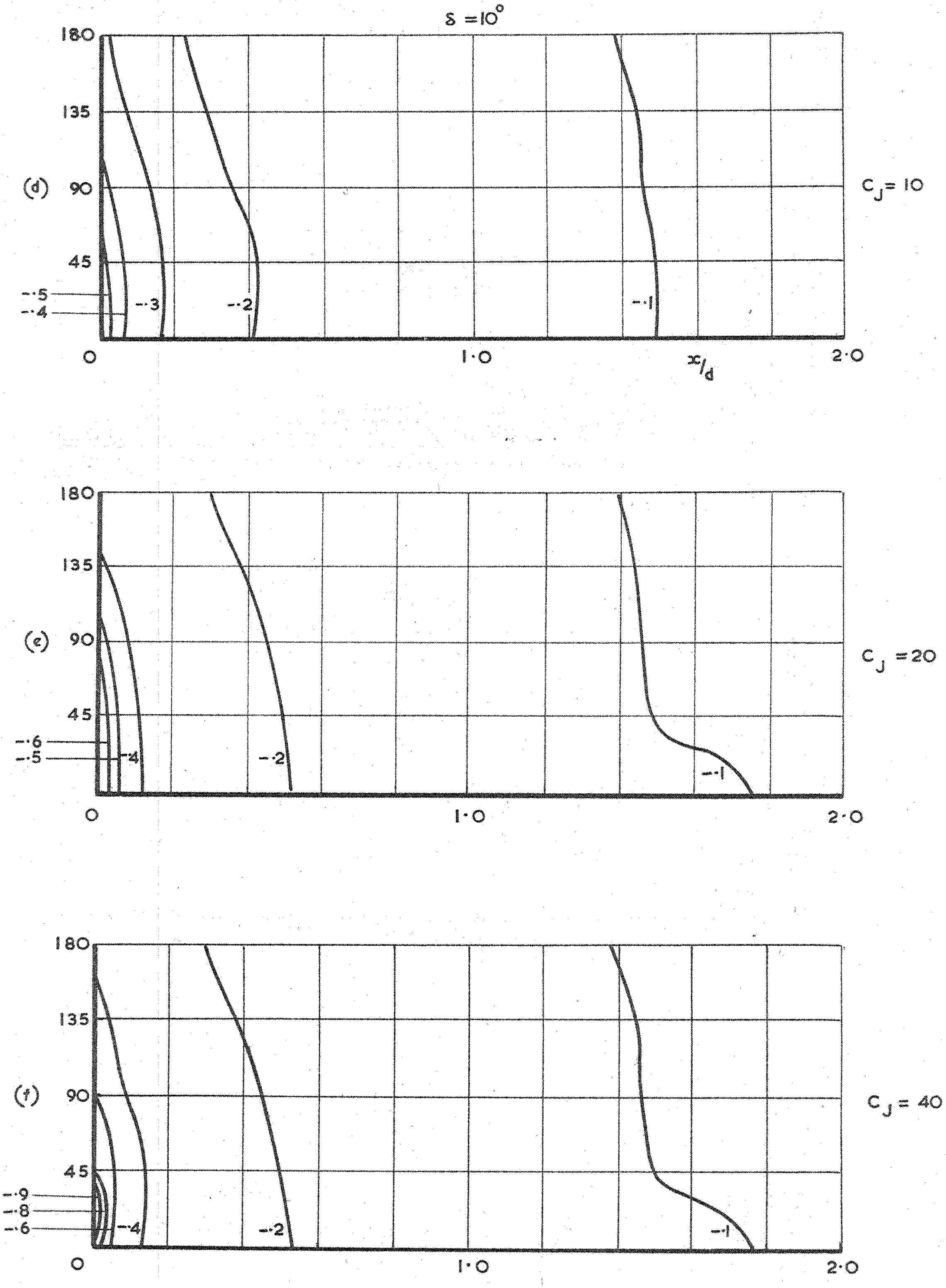

FIG. 5. SIDE PRESSURE DISTIBUTIONS

TABLE II. (Cont) Base Suction Coefficients for 5° jet deflection

θ	C_J \ $\frac{r}{R}$	0.237	0.287	0.337	0.387	0.437	0.487	0.537	0.587	0.637	0.687	0.737	0.787	0.837	0.887	0.937
$\theta = 135^{\circ}$	0	0.165	0.165	0.163	0.163	0.165	0.165	0.165	0.167	0.167	0.167	0.165	0.165	0.165	0.165	0.165
	1	0.259	0.263	0.269	0.284	0.302	0.314	0.309	0.316	0.322	0.327	0.324	0.324	0.308	0.294	0.276
	2	0.287	0.285	0.296	0.302	0.318	0.336	0.347	0.345	0.358	0.358	0.362	0.365	0.343	0.318	0.294
	4	0.283	0.288	0.292	0.309	0.337	0.389	0.432	0.452	0.484	0.500	0.503	0.498	0.452	0.397	0.359
	6	0.274	0.267	0.275	0.307	0.365	0.445	0.485	0.520	0.546	0.582	0.578	0.532	0.506	0.432	0.376
	8	0.269	0.275	0.283	0.335	0.402	0.472	0.526	0.574	0.583	0.605	0.596	0.574	0.541	0.460	0.412
	10	0.285	0.285	0.308	0.376	0.434	0.507	0.584	0.631	0.637	0.621	0.642	0.638	0.609	0.548	0.473
	15	0.316	0.324	0.347	0.440	0.516	0.598	0.649	0.716	0.729	0.743	0.735	0.735	0.697	0.626	0.554
	20	0.358	0.362	0.380	0.438	0.537	0.612	0.713	0.772	0.801	0.848	0.852	0.829	0.765	0.694	0.619
	25	0.372	0.378	0.394	0.444	0.543	0.624	0.745	0.829	0.845	0.894	0.889	0.856	0.807	0.722	0.637
	30	0.391	0.382	0.404	0.448	0.546	0.639	0.762	0.843	0.868	0.913	0.916	0.903	0.846	0.765	0.702
	35	0.406	0.418	0.429	0.452	0.559	0.644	0.779	0.882	0.902	0.936	0.930	0.928	0.864	0.781	0.718
	40	0.437	0.437	0.437	0.465	0.574	0.676	0.784	0.909	0.916	0.948	0.945	0.940	0.902	0.815	0.746
$\theta = 157\frac{1}{2}^{\circ}$	0	0.163	0.165	0.165	0.165	0.163	0.163	0.165	0.165	0.167	0.167	0.167	0.165	0.165	0.165	0.165
	1	0.248	0.248	0.250	0.258	0.274	0.287	0.287	0.296	0.296	0.294	0.290	0.283	0.279	0.272	0.265
	2	0.260	0.257	0.263	0.276	0.285	0.298	0.306	0.318	0.322	0.325	0.325	0.318	0.315	0.310	0.298
	4	0.260	0.264	0.268	0.279	0.297	0.320	0.342	0.385	0.415	0.432	0.436	0.402	0.384	0.364	0.330
	6	0.265	0.260	0.268	0.293	0.321	0.348	0.395	0.476	0.501	0.519	0.510	0.497	0.446	0.418	0.349
	8	0.256	0.256	0.263	0.312	0.349	0.383	0.458	0.513	0.529	0.533	0.542	0.528	0.489	0.434	0.367
	10	0.263	0.263	0.274	0.324	0.372	0.436	0.529	0.564	0.587	0.601	0.618	0.576	0.532	0.482	0.403
	15	0.312	0.305	0.310	0.358	0.418	0.489	0.571	0.677	0.674	0.714	0.728	0.693	0.651	0.594	0.518
	20	0.339	0.328	0.336	0.395	0.476	0.531	0.654	0.768	0.783	0.798	0.786	0.731	0.693	0.652	0.582
	25	0.346	0.342	0.354	0.417	0.503	0.566	0.705	0.826	0.850	0.886	0.873	0.815	0.734	0.687	0.625
	30	0.365	0.365	0.373	0.439	0.500	0.584	0.726	0.860	0.872	0.901	0.890	0.854	0.775	0.721	0.688
	35	0.380	0.374	0.379	0.442	0.518	0.590	0.741	0.882	0.907	0.913	0.913	0.862	0.798	0.748	0.706
	40	0.402	0.402	0.427	0.456	0.524	0.615	0.748	0.916	0.921	0.921	0.918	0.889	0.826	0.784	0.732
$\theta = 180^{\circ}$	0	0.165	0.165	0.167	0.167	0.165	0.165	0.165	0.167	0.165	0.165	0.163	0.163	0.163	0.165	0.163
	1	0.245	0.245	0.250	0.258	0.267	0.267	0.273	0.285	0.282	0.287	0.285	0.271	0.264	0.266	0.260
	2	0.245	0.245	0.256	0.267	0.277	0.283	0.286	0.291	0.296	0.309	0.309	0.306	0.300	0.300	0.285
	4	0.229	0.222	0.234	0.255	0.272	0.278	0.298	0.345	0.372	0.396	0.392	0.375	0.365	0.342	0.330
	6	0.217	0.222	0.230	0.261	0.279	0.329	0.357	0.406	0.461	0.483	0.478	0.454	0.427	0.396	0.342
	8	0.236	0.236	0.247	0.293	0.342	0.396	0.412	0.452	0.507	0.551	0.551	0.523	0.476	0.420	0.369
	10	0.254	0.254	0.269	0.314	0.375	0.465	0.498	0.549	0.584	0.620	0.615	0.579	0.513	0.446	0.416
	15	0.269	0.275	0.288	0.338	0.398	0.479	0.549	0.618	0.663	0.704	0.697	0.654	0.602	0.578	0.523
	20	0.287	0.287	0.302	0.362	0.411	0.526	0.574	0.703	0.748	0.765	0.753	0.690	0.638	0.613	0.597
	25	0.306	0.306	0.315	0.385	0.430	0.538	0.589	0.746	0.802	0.843	0.829	0.758	0.706	0.651	0.634
	30	0.332	0.330	0.348	0.417	0.446	0.561	0.647	0.758	0.859	0.876	0.882	0.805	0.759	0.714	0.693
	35	0.367	0.367	0.382	0.442	0.455	0.580	0.662	0.765	0.886	0.918	0.918	0.837	0.786	0.746	0.706
	40	0.374	0.374	0.396	0.448	0.469	0.592	0.671	0.771	0.902	0.930	0.905	0.873	0.817	0.773	0.721

TABLE II. (Cont) Base Suction Coefficients for 5° jet deflection

θ	C_J \ $\frac{r}{R}$	0.237	0.287	0.337	0.387	0.437	0.487	0.537	0.587	0.637	0.687	0.737	0.787	0.837	0.887	0.937
$\theta = 67\frac{1}{2}^{\circ}$	0	0.165	0.165	0.165	0.165	0.165	0.167	0.169	0.167	0.169	0.165	0.165	0.165	0.165	0.165	0.165
	1	0.308	0.312	0.316	0.328	0.331	0.331	0.328	0.335	0.337	0.341	0.338	0.338	0.326	0.320	0.313
	2	0.335	0.332	0.335	0.358	0.376	0.385	0.402	0.428	0.456	0.448	0.442	0.425	0.401	0.387	0.356
	4	0.378	0.378	0.385	0.432	0.486	0.507	0.553	0.589	0.574	0.586	0.592	0.551	0.527	0.483	0.450
	6	0.395	0.397	0.402	0.448	0.503	0.576	0.607	0.659	0.662	0.648	0.659	0.612	0.573	0.540	0.502
	8	0.439	0.439	0.442	0.486	0.539	0.607	0.654	0.703	0.696	0.707	0.728	0.684	0.623	0.578	0.552
	10	0.472	0.476	0.484	0.532	0.586	0.673	0.735	0.754	0.766	0.757	0.752	0.729	0.668	0.639	0.572
	15	0.492	0.487	0.503	0.562	0.665	0.723	0.776	0.842	0.884	0.878	0.896	0.862	0.791	0.753	0.675
	20	0.512	0.517	0.528	0.594	0.656	0.773	0.847	0.896	0.945	0.972	0.998	0.957	0.916	0.824	0.751
	25	0.522	0.518	0.547	0.646	0.717	0.822	0.903	0.965	1.058	1.076	1.063	1.032	0.997	0.891	0.788
	30	0.554	0.554	0.603	0.672	0.748	0.864	0.942	1.036	1.078	1.109	1.105	1.056	0.972	0.931	0.828
	35	0.593	0.598	0.642	0.731	0.804	0.907	1.028	1.076	1.102	1.149	1.156	1.122	1.018	0.947	0.862
	40	0.625	0.632	0.706	0.794	0.887	0.962	1.076	1.153	1.198	1.246	1.238	1.196	1.084	0.992	0.897
$\theta = 90^{\circ}$	0	0.163	0.163	0.165	0.165	0.167	0.167	0.165	0.165	0.165	0.165	0.165	0.165	0.165	0.165	0.165
	1	0.306	0.306	0.313	0.327	0.330	0.335	0.342	0.357	0.359	0.348	0.357	0.350	0.342	0.336	0.318
	2	0.327	0.330	0.338	0.353	0.356	0.382	0.438	0.449	0.456	0.463	0.458	0.427	0.412	0.376	0.354
	4	0.368	0.374	0.370	0.396	0.448	0.507	0.556	0.584	0.588	0.603	0.616	0.579	0.543	0.478	0.432
	6	0.357	0.348	0.370	0.418	0.457	0.529	0.578	0.647	0.639	0.648	0.657	0.646	0.589	0.521	0.473
	8	0.389	0.392	0.396	0.448	0.493	0.542	0.638	0.686	0.693	0.672	0.688	0.645	0.598	0.554	0.487
	10	0.402	0.397	0.418	0.464	0.552	0.607	0.679	0.718	0.724	0.715	0.732	0.716	0.673	0.611	0.547
	15	0.430	0.438	0.476	0.527	0.605	0.628	0.773	0.849	0.927	0.856	0.892	0.865	0.759	0.718	0.634
	20	0.463	0.459	0.495	0.563	0.627	0.728	0.854	0.873	0.954	1.018	0.992	0.954	0.886	0.810	0.725
	25	0.516	0.522	0.548	0.613	0.696	0.802	0.896	0.913	0.994	1.054	1.036	1.024	0.937	0.832	0.757
	30	0.548	0.542	0.567	0.635	0.710	0.836	0.902	1.016	1.054	1.078	1.076	1.057	0.968	0.894	0.787
	35	0.567	0.562	0.584	0.639	0.723	0.887	0.956	1.082	1.138	1.148	1.130	1.082	1.006	0.925	0.834
	40	0.596	0.587	0.662	0.748	0.826	0.924	1.035	1.109	1.158	1.197	1.158	1.132	1.046	0.963	0.815
$\theta = 112\frac{1}{2}^{\circ}$	0	0.167	0.167	0.167	0.165	0.165	0.167	0.163	0.163	0.163	0.165	0.165	0.165	0.165	0.165	0.165
	1	0.287	0.285	0.285	0.293	0.298	0.306	0.315	0.333	0.342	0.338	0.338	0.327	0.324	0.317	0.303
	2	0.326	0.320	0.322	0.327	0.348	0.354	0.372	0.386	0.394	0.413	0.437	0.420	0.411	0.386	0.354
	4	0.334	0.340	0.338	0.365	0.420	0.467	0.483	0.529	0.529	0.546	0.532	0.504	0.466	0.431	0.382
	6	0.334	0.328	0.328	0.365	0.428	0.496	0.553	0.587	0.572	0.599	0.616	0.544	0.503	0.466	0.412
	8	0.357	0.362	0.362	0.398	0.466	0.517	0.579	0.612	0.638	0.649	0.627	0.593	0.552	0.486	0.440
	10	0.356	0.360	0.368	0.412	0.487	0.543	0.628	0.659	0.686	0.702	0.726	0.678	0.627	0.576	0.514
	15	0.376	0.384	0.412	0.486	0.579	0.612	0.697	0.784	0.793	0.798	0.827	0.804	0.726	0.668	0.593
	20	0.403	0.400	0.438	0.517	0.602	0.708	0.773	0.864	0.908	0.937	0.919	0.895	0.827	0.762	0.678
	25	0.412	0.408	0.443	0.527	0.608	0.715	0.823	0.896	0.952	0.973	0.985	0.954	0.853	0.766	0.707
	30	0.448	0.440	0.452	0.537	0.618	0.734	0.852	0.938	0.983	1.031	0.988	0.934	0.867	0.801	0.723
	35	0.468	0.465	0.465	0.572	0.678	0.794	0.907	0.998	1.047	1.054	1.048	1.006	0.947	0.832	0.746
	40	0.497	0.502	0.538	0.577	0.703	0.805	0.976	1.038	1.054	1.097	1.102	1.066	1.003	0.898	0.767

TABLE II. Base Suction Coefficients for 5° jet deflection

	C_J \ $\frac{r}{R}$	0.237	0.287	0.337	0.387	0.437	0.487	0.537	0.587	0.637	0.687	0.737	0.787	0.837	0.887	0.937
$\theta = 0^{\circ}$	0	0.165	0.165	0.165	0.163	0.165	0.165	0.165	0.165	0.163	0.167	0.165	0.165	0.165	0.165	0.165
	1	0.286	0.296	0.302	0.316	0.322	0.322	0.328	0.347	0.356	0.368	0.364	0.358	0.356	0.348	0.342
	2	0.293	0.302	0.302	0.342	0.396	0.427	0.427	0.444	0.458	0.458	0.444	0.436	0.427	0.416	0.410
	4	0.342	0.346	0.467	0.414	0.427	0.486	0.504	0.538	0.527	0.555	0.553	0.528	0.504	0.478	0.452
	6	0.402	0.406	0.412	0.437	0.465	0.531	0.592	0.662	0.654	0.615	0.676	0.643	0.620	0.556	0.496
	8	0.444	0.453	0.456	0.472	0.504	0.601	0.663	0.711	0.742	0.750	0.764	0.731	0.702	0.638	0.564
	10	0.467	0.462	0.472	0.496	0.563	0.684	0.746	0.804	0.815	0.812	0.828	0.796	0.748	0.703	0.654
	15	0.500	0.496	0.496	0.547	0.622	0.720	0.797	0.873	0.878	0.856	0.902	0.898	0.862	0.812	0.728
	20	0.528	0.522	0.534	0.602	0.660	0.797	0.832	0.915	0.988	0.988	1.000	0.975	0.947	0.894	0.846
	25	0.546	0.535	0.540	0.641	0.764	0.826	0.904	0.988	1.047	1.054	1.121	1.054	1.002	0.957	0.915
	30	0.583	0.596	0.657	0.736	0.816	0.942	0.975	1.016	1.096	1.121	1.187	1.104	1.054	1.000	0.959
	35	0.615	0.624	0.693	0.782	0.867	0.983	1.047	1.104	1.121	1.187	1.274	1.194	1.104	1.064	1.021
	40	0.624	0.661	0.738	0.836	0.920	1.002	1.084	1.156	1.163	1.249	1.322	1.278	1.220	1.158	1.093
$\theta = 22\frac{1}{2}^{\circ}$	0	0.165	0.163	0.163	0.165	0.165	0.167	0.167	0.167	0.169	0.169	0.165	0.165	0.165	0.165	0.165
	1	0.284	0.284	0.289	0.316	0.332	0.332	0.350	0.356	0.365	0.380	0.376	0.352	0.358	0.334	0.297
	2	0.365	0.373	0.402	0.397	0.401	0.426	0.458	0.507	0.523	0.564	0.531	0.506	0.487	0.458	0.394
	4	0.368	0.372	0.406	0.448	0.487	0.512	0.578	0.612	0.572	0.578	0.582	0.546	0.502	0.498	0.476
	6	0.407	0.405	0.410	0.486	0.529	0.583	0.626	0.684	0.678	0.693	0.702	0.654	0.627	0.588	0.519
	8	0.457	0.453	0.464	0.547	0.552	0.638	0.706	0.738	0.702	0.778	0.767	0.734	0.700	0.648	0.603
	10	0.512	0.516	0.510	0.548	0.617	0.692	0.759	0.802	0.813	0.824	0.820	0.763	0.724	0.696	0.650
	15	0.526	0.526	0.531	0.594	0.648	0.752	0.796	0.829	0.884	0.902	0.916	0.882	0.827	0.794	0.723
	20	0.534	0.528	0.556	0.632	0.717	0.813	0.885	0.926	0.998	1.013	1.010	0.984	0.937	0.862	0.796
	25	0.554	0.548	0.548	0.651	0.772	0.865	0.913	0.988	1.036	1.068	1.064	1.039	0.992	0.918	0.850
	30	0.576	0.576	0.576	0.648	0.794	0.913	0.978	1.021	1.103	1.128	1.103	1.072	1.039	0.976	0.903
	35	0.582	0.582	0.661	0.735	0.874	0.948	1.039	1.103	1.142	1.176	1.169	1.183	1.078	1.014	0.943
	40	0.607	0.651	0.732	0.806	0.915	0.993	1.114	1.151	1.224	1.238	1.203	1.203	1.132	1.106	1.004
$\theta = 45^{\circ}$	0	0.163	0.163	0.165	0.165	0.167	0.169	0.165	0.165	0.169	0.165	0.161	0.161	0.165	0.165	0.165
	1	0.307	0.307	0.315	0.326	0.334	0.347	0.352	0.368	0.365	0.382	0.374	0.356	0.338	0.312	0.297
	2	0.348	0.348	0.365	0.407	0.412	0.448	0.462	0.493	0.497	0.464	0.492	0.458	0.406	0.393	0.372
	4	0.403	0.408	0.413	0.457	0.502	0.553	0.588	0.596	0.631	0.622	0.598	0.554	0.527	0.498	0.472
	6	0.438	0.434	0.452	0.476	0.548	0.613	0.647	0.675	0.688	0.693	0.672	0.654	0.587	0.543	0.528
	8	0.456	0.458	0.467	0.543	0.602	0.686	0.705	0.743	0.758	0.742	0.721	0.697	0.643	0.598	0.554
	10	0.486	0.482	0.527	0.584	0.673	0.752	0.786	0.788	0.822	0.813	0.796	0.768	0.703	0.687	0.613
	15	0.524	0.528	0.536	0.612	0.676	0.793	0.798	0.837	0.892	0.916	0.928	0.903	0.872	0.794	0.718
	20	0.538	0.538	0.594	0.667	0.738	0.804	0.888	0.968	1.028	1.046	1.039	1.002	0.936	0.854	0.817
	25	0.564	0.558	0.602	0.679	0.750	0.856	0.927	1.014	1.078	1.122	1.067	1.023	0.994	0.906	0.869
	30	0.598	0.596	0.632	0.704	0.796	0.953	1.014	1.068	1.102	1.135	1.130	1.119	1.026	0.954	0.887
	35	0.648	0.645	0.693	0.784	0.867	0.976	1.122	1.148	1.165	1.199	1.204	1.164	1.027	0.986	0.893
	40	0.667	0.660	0.762	0.848	0.957	1.123	1.186	1.188	1.254	1.276	1.289	1.212	1.104	1.032	0.927

TABLE I. (Cont). Base Suction Coefficients for 2° jet deflection

θ	$\frac{r}{R}$ / C_J	0.237	0.287	0.337	0.387	0.437	0.487	0.537	0.587	0.637	0.687	0.737	0.787	0.837	0.887	0.937
$\theta = 135^{\circ}$	0	0.165	0.165	0.165	0.165	0.165	0.165	0.165	0.165	0.165	0.165	0.165	0.165	0.165	0.165	0.165
	1	0.235	0.218	0.216	0.224	0.228	0.232	0.238	0.246	0.254	0.254	0.248	0.244	0.242	0.230	0.218
	2	0.282	0.276	0.282	0.293	0.324	0.340	0.362	0.348	0.326	0.354	0.358	0.350	0.347	0.328	0.292
	4	0.282	0.276	0.282	0.328	0.402	0.498	0.532	0.532	0.565	0.582	0.563	0.518	0.496	0.448	0.392
	6	0.282	0.276	0.282	0.328	0.402	0.527	0.583	0.602	0.643	0.647	0.626	0.588	0.532	0.481	0.413
	8	0.300	0.282	0.304	0.362	0.479	0.562	0.620	0.622	0.662	0.658	0.638	0.602	0.556	0.507	0.432
	10	0.342	0.348	0.382	0.437	0.510	0.618	0.683	0.698	0.687	0.776	0.784	0.737	0.676	0.622	0.558
	15	0.482	0.478	0.509	0.600	0.678	0.756	0.829	0.891	0.827	0.891	0.912	0.895	0.826	0.761	0.724
	20	0.512	0.521	0.548	0.612	0.700	0.792	0.890	0.962	1.100	1.100	1.046	0.982	0.928	0.861	0.813
	25	0.547	0.538	0.565	0.628	0.718	0.823	0.951	1.032	1.121	1.135	1.078	1.016	0.948	0.879	0.842
	30	0.578	0.550	0.582	0.643	0.731	0.892	1.032	1.096	1.166	1.158	1.113	1.045	0.962	0.898	0.862
	35	0.632	0.600	0.600	0.661	0.792	0.978	1.127	1.216	1.213	1.210	1.237	1.169	1.082	0,998	0.927
	40	0.686	0.635	0.632	0.680	0.882	1.063	1.231	1.305	1.238	1.231	1.372	1.302	1.186	1.100	0.965
$\theta = 157\frac{1}{2}$	0	0.165	0.165	0.163	0.163	0.163	0.165	0.163	0.165	0.165	0.165	0.167	0.167	0.167	0.165	0.165
	1	0.216	0.216	0.216	0.224	0.228	0.232	0.238	0.240	0.243	0.248	0.248	0.245	0.242	0.230	0.218
	2	0.251	0.248	0.248	0.267	0.289	0.306	0.302	0.297	0.302	0.316	0.329	0.326	0.320	0.306	0.281
	4	0.267	0.263	0.276	0.309	0.324	0.378	0.416	0.432	0.467	0.501	0.516	0.471	0.457	0.412	0.357
	6	0.284	0.297	0.302	0.328	0.347	0.404	0.492	0.534	0.571	0.583	0.585	0.562	0.513	0.457	0.385
	8	0.300	0.307	0.326	0.397	0.465	0.512	0.526	0.571	0.613	0.624	0.622	0.586	0.524	0.468	0.388
	10	0.348	0.342	0.406	0.443	0.510	0.553	0.626	0.650	0.685	0.728	0.707	0.654	0.602	0.541	0.473
	15	0.436	0.445	0.481	0.546	0.603	0.677	0.751	0.813	0.811	0.834	0.861	0.837	0.783	0.720	0.662
	20	0.496	0.502	0.517	0.576	0.654	0.781	0.902	0.987	1.086	1.066	1.025	0.939	0.894	0.833	0.784
	25	0.518	0.527	0.550	0.605	0.697	0.804	0.947	1.046	1.098	1.098	1.066	1.002	0.930	0.863	0.811
	30	0.569	0.564	0.587	0.637	0.728	0.837	0.988	1.067	1.142	1.037	1.084	1.045	0.962	0.892	0.825
	35	0.603	0.603	0.619	0.668	0.780	0.925	1.094	1.194	1.194	1.181	1.194	1.098	1.057	0.951	0.883
	40	0.642	0.635	0.630	0.694	0.834	0.993	1.128	1.213	1.247	1.224	1.273	1.194	1.088	1.032	0.907
$\theta = 180^{\circ}$	0	0.165	0.165	0.165	0.165	0.165	0.165	0.165	0.165	0.165	0.165	0.165	0.165	0.165	0.165	0.165
	1	0.211	0.216	0.221	0.224	0.216	0.232	0.238	0.238	0.232	0.241	0.238	0.241	0.241	0.232	0.221
	2	0.240	0.248	0.248	0.252	0.248	0.242	0.242	0.267	0.282	0.300	0.309	0.318	0.313	0.300	0.278
	4	0.240	0.258	0.278	0.295	0.278	0.272	0.338	0.382	0.415	0.452	0.467	0.452	0.438	0.392	0.333
	6	0.280	0.303	0.328	0.328	0.298	0.342	0.415	0.482	0.520	0.558	0.563	0.558	0.502	0.435	0.356
	8	0.310	0.345	0.382	0.436	0.495	0.473	0.458	0.522	0.565	0.609	0.612	0.574	0.511	0.450	0.365
	10	0.342	0.381	0.435	0.482	0.516	0.520	0.573	0.631	0.675	0.712	0.680	0.622	0.558	0.492	0.423
	15	0.418	0.440	0.468	0.512	0.558	0.613	0.702	0.762	0.809	0.827	0.823	0.792	0.753	0.690	0.632
	20	0.482	0.482	0.491	0.543	0.628	0.773	0.891	0.972	1.025	1.054	1.018	0.962	0.891	0.825	0.767
	25	0.515	0.523	0.540	0.595	0.682	0.796	0.920	1.013	1.072	1.084	1.059	0.998	0.930	0.858	0.792
	30	0.561	0.561	0.582	0.641	0.739	0.835	0.958	1.072	1.123	1.118	1.079	1.032	0.961	0.890	0.825
	35	0.590	0.586	0.612	0.682	0.787	0.901	1.032	1.146	1.202	1.208	1.149	1.070	0.992	0.930	0.857
	40	0.625	0.620	0.641	0.722	0.828	0.963	1.094	1.202	1.298	1.305	1.237	1.116	1.032	0.964	0.893

TABLE I. (Cont) Base Suction Coefficients for 2° jet deflection

θ	C_J \ $\frac{r}{R}$	0.237	0.287	0.337	0.387	0.437	0.487	0.537	0.587	0.637	0.687	0.737	0.787	0.837	0.887	0.937
$\theta = 67\frac{1}{2}^{\circ}$	0	0.165	0.165	0.163	0.165	0.165	0.165	0.167	0.167	0.167	0.169	0.165	0.165	0.165	0.163	0.165
	1	0.256	0.268	0.273	0.284	0.288	0.293	0.307	0.302	0.302	0.291	0.296	0.296	0.291	0.285	0.282
	2	0.305	0.316	0.338	0.356	0.369	0.402	0.434	0.437	0.428	0.431	0.439	0.418	0.396	0.371	0.339
	4	0.318	0.322	0.376	0.438	0.491	0.539	0.572	0.615	0.611	0.634	0.634	0.596	0.552	0.500	0.451
	6	0.339	0.342	0.384	0.440	0.536	0.607	0.645	0.676	0.678	0.669	0.647	0.621	0.577	0.545	0.512
	8	0.356	0.369	0.415	0.477	0.548	0.621	0.684	0.711	0.726	0.726	0.734	0.689	0.645	0.586	0.547
	10	0.402	0.402	0.437	0.528	0.635	0.710	0.762	0.785	0.796	0.774	0.774	0.738	0.679	0.640	0.593
	15	0.441	0.437	0.508	0.576	0.672	0.738	0.795	0.854	0.920	0.917	0.908	0.884	0.836	0.784	0.702
	20	0.469	0.469	0.525	0.586	0.692	0.837	0.906	0.927	0.993	1.032	1.044	1.000	0.957	0.882	0.803
	25	0.534	0.534	0.600	0.689	0.756	0.918	0.989	1.034	1.115	1.142	1.109	1.106	1.083	0.976	0.875
	30	0.582	0.587	0.628	0.701	0.783	0.942	1.038	1.127	1.165	1.187	1.174	1.106	1.047	0.957	0.900
	35	0.669	0.667	0.742	0.811	0.897	1.032	1.146	1.184	1.237	1.237	1.268	1.195	1.096	1.019	0.953
	40	0.728	0.732	0.818	0.924	1.009	1.103	1.254	1.316	1.372	1.374	1.362	1.309	1.142	1.083	1.005
$\theta = 90^{\circ}$	0	0.165	0.165	0.165	0.165	0.163	0.163	0.165	0.165	0.165	0.165	0.165	0.165	0.167	0.165	0.165
	1	0.254	0.261	0.261	0.266	0.266	0.273	0.291	0.296	0.288	0.286	0.292	0.296	0.278	0.265	0.254
	2	0.291	0.302	0.316	0.329	0.348	0.367	0.422	0.448	0.422	0.426	0.451	0.432	0.414	0.362	0.333
	4	0.322	0.328	0.356	0.412	0.463	0.525	0.596	0.618	0.607	0.634	0.642	0.600	0.566	0.514	0.451
	6	0.333	0.342	0.371	0.422	0.465	0.542	0.620	0.668	0.674	0.652	0.676	0.662	0.618	0.562	0.510
	8	0.343	0.355	0.391	0.440	0.496	0.561	0.654	0.707	0.736	0.722	0.720	0.689	0.641	0.592	0.526
	10	0.373	0.373	0.411	0.508	0.602	0.672	0.740	0.767	0.780	0.762	0.797	0.763	0.714	0.652	0.583
	15	0.436	0.439	0.502	0.580	0.672	0.669	0.861	0.918	0.916	0.862	0.901	0.872	0.825	0.764	0.691
	20	0.480	0.472	0.525	0.618	0.730	0.859	0.958	0.918	1.058	1.127	1.085	1.036	0.972	0.908	0.850
	25	0.547	0.552	0.600	0.669	0.770	0.902	0.991	0.991	1.083	1.138	1.106	1.062	1.003	0.928	0.872
	30	0.608	0.622	0.651	0.728	0.811	0.952	1.027	1.120	1.161	1.159	1.122	1.096	1.032	0.961	0.895
	35	0.669	0.702	0.761	0.825	0.912	1.016	1.125	1.208	1.262	1.262	1.230	1.178	1.128	1.033	0.947
	40	0.746	0.792	0.851	0.922	1.018	1.112	1.228	1.332	1.368	1.368	1.332	1.300	1.182	1.110	1.028
$\theta = 112\frac{1}{2}^{\circ}$	0	0.165	0.165	0.165	0.165	0.163	0.163	0.163	0.163	0.165	0.165	0.165	0.165	0.165	0.165	0.165
	1	0.242	0.237	0.237	0.248	0.251	0.256	0.265	0.273	0.265	0.269	0.262	0.258	0.247	0.236	0.222
	2	0.285	0.280	0.280	0.306	0.331	0.349	0.384	0.392	0.367	0.376	0.400	0.386	0.371	0.340	0.307
	4	0.296	0.296	0.312	0.365	0.427	0.505	0.557	0.571	0.580	0.603	0.598	0.551	0.498	0.457	0.409
	6	0.318	0.321	0.327	0.368	0.444	0.542	0.596	0.627	0.651	0.647	0.647	0.613	0.564	0.511	0.442
	8	0.327	0.325	0.336	0.392	0.479	0.562	0.631	0.648	0.687	0.687	0.675	0.637	0.592	0.538	0.474
	10	0.351	0.348	0.374	0.459	0.546	0.637	0.712	0.725	0.725	0.742	0.789	0.742	0.683	0.635	0.566
	15	0.452	0.448	0.507	0.582	0.672	0.694	0.789	0.886	0.864	0.868	0.894	0.888	0.836	0.753	0.703
	20	0.490	0.493	0.528	0.605	0.708	0.816	0.914	0.964	1.037	1.076	1.053	1.009	0.942	0.876	0.805
	25	0.526	0.531	0.565	0.637	0.735	0.851	0.967	1.018	1.096	1.138	1.106	1.045	0.979	0.899	0.854
	30	0.584	0.584	0.612	0.673	0.764	0.917	1.018	1.102	1.165	1.159	1.113	1.064	0.992	0.927	0.886
	35	0.643	0.646	0.665	0.726	0.846	0.993	1.109	1.224	1.238	1.227	1.237	1.143	1.074	1.006	0.931
	40	0.699	0.697	0.704	0.741	0.916	1.102	1.258	1.289	1.274	1.284	1.358	1.299	1.189	1.109	0.997

TABLE I. Base Suction Coefficients for 2° jet deflection

θ	C_J \ $\frac{r}{R}$	0.237	0.287	0.337	0.387	0.437	0.487	0.537	0.587	0.637	0.687	0.737	0.787	0.837	0.887	0.937
θ=0°	0	0.163	0.165	0.165	0.165	0.163	0.165	0.165	0.165	0.165	0.167	0.167	0.165	0.165	0.165	0.165
	1	0.286	0.282	0.282	0.293	0.310	0.332	0.359	0.371	0.362	0.380	0.378	0.351	0.359	0.332	0.287
	2	0.286	0.286	0.293	0.322	0.353	0.388	0.417	0.415	0.421	0.436	0.412	0.416	0.390	0.378	0.330
	4	0.286	0.286	0.293	0.322	0.370	0.427	0.480	0.480	0.538	0.569	0.567	0.532	0.500	0.452	0.408
	6	0.293	0.293	0.302	0.341	0.388	0.487	0.538	0.567	0.615	0.602	0.609	0.583	0.542	0.500	0.427
	8	0.293	0.293	0.302	0.388	0.375	0.622	0.673	0.670	0.682	0.709	0.698	0.661	0.638	0.564	0.521
	10	0.296	0.310	0.353	0.423	0.552	0.698	0.722	0.709	0.802	0.791	0.765	0.728	0.679	0.618	0.546
	15	0.302	0.322	0.388	0.482	0.625	0.797	0.827	0.903	0.962	0.962	0.944	0.890	0.826	0.754	0.686
	20	0.302	0.322	0.408	0.543	0.709	0.827	0.903	1.000	1.074	1.072	1.043	1.028	0.962	0.881	0.818
	25	0.347	0.375	0.465	0.583	0.765	0.962	0.962	1.024	1.161	1.161	1.212	1.112	1.028	0.944	0.849
	30	0.341	0.412	0.482	0.602	0.797	1.034	1.038	1.043	1.237	1.241	1.237	1.168	1.096	0.986	0.892
	35	0.495	0.584	0.615	0.765	0.884	1.052	1.106	1.161	1.248	1.312	1.312	1.236	1.154	1.058	1.000
	40	0.602	0.650	0.738	0.849	0.956	1.058	1.161	1.212	1.241	1.368	1.392	1.318	1.256	1.188	1.112
θ=22½°	0	0.165	0.165	0.163	0.163	0.165	0.165	0.165	0.169	0.169	0.167	0.165	0.165	0.163	0.163	0.163
	1	0.286	0.286	0.286	0.298	0.310	0.326	0.344	0.344	0.317	0.367	0.358	0.336	0.327	0.302	0.274
	2	0.286	0.286	0.315	0.356	0.368	0.407	0.426	0.438	0.425	0.442	0.420	0.402	0.388	0.378	0.330
	4	0.292	0.286	0.324	0.373	0.407	0.486	0.514	0.526	0.532	0.558	0.572	0.546	0.502	0.464	0.413
	6	0.307	0.300	0.356	0.402	0.462	0.542	0.573	0.583	0.642	0.620	0.603	0.594	0.542	0.506	0.441
	8	0.327	0.325	0.378	0.437	0.496	0.622	0.684	0.701	0.716	0.705	0.684	0.653	0.638	0.564	0.521
	10	0.353	0.360	0.413	0.476	0.574	0.704	0.736	0.736	0.810	0.810	0.765	0.732	0.675	0.627	0.563
	15	0.386	0.386	0.442	0.534	0.637	0.765	0.802	0.847	0.928	0.962	0.921	0.874	0.831	0.764	0.699
	20	0.397	0.402	0.496	0.580	0.702	0.839	0.917	0.998	1.036	1.096	1.068	1.036	0.958	0.881	0.784
	25	0.426	0.437	0.522	0.626	0.765	0.891	0.954	1.021	1.098	1.134	1.096	1.061	1.024	0.944	0.849
	30	0.444	0.496	0.547	0.673	0.822	0.976	1.038	1.064	1.182	1.226	1.147	1.102	1.068	0.986	0.917
	35	0.460	0.552	0.648	0.708	0.896	1.028	1.114	1.195	1.237	1.268	1.206	1.212	1.123	1.058	1.000
	40	0.507	0.628	0.756	0.837	0.983	1.060	1.203	1.203	1.318	1.384	1.268	1.286	1.216	1.168	1.094
θ = 45°	0	0.165	0.165	0.165	0.165	0.165	0.163	0.165	0.165	0.165	0.165	0.163	0.165	0.165	0.165	0.165
	1	0.262	0.273	0.289	0.302	0.326	0.332	0.332	0.326	0.309	0.309	0.298	0.302	0.298	0.287	0.287
	2	0.310	0.332	0.365	0.402	0.398	0.463	0.465	0.447	0.442	0.442	0.427	0.413	0.388	0.392	0.356
	4	0.322	0.322	0.382	0.444	0.511	0.566	0.602	0.602	0.633	0.631	0.609	0.572	0.535	0.496	0.465
	6	0.350	0.356	0.417	0.462	0.557	0.638	0.662	0.662	0.686	0.673	0.650	0.616	0.560	0.538	0.515
	8	0.382	0.396	0.462	0.535	0.613	0.704	0.723	0.726	0.759	0.737	0.708	0.673	0.622	0.575	0.556
	10	0.446	0.446	0.529	0.578	0.683	0.771	0.790	0.790	0.838	0.822	0.785	0.746	0.675	0.632	0.584
	15	0.463	0.468	0.524	0.582	0.687	0.825	0.825	0.862	0.925	0.962	0.962	0.937	0.894	0.800	0.725
	20	0.480	0.496	0.603	0.674	0.756	0.868	0.954	1.032	1.096	1.116	1.100	1.068	0.987	0.893	0.857
	25	0.512	0.522	0.609	0.686	0.759	0.921	0.983	1.096	1.122	1.161	1.112	1.096	1.024	0.944	0.881
	30	0.576	0.572	0.618	0.685	0.762	0.990	1.096	1.102	1.165	1.172	1.168	1.127	1.043	0.963	0.912
	35	0.667	0.685	0.737	0.806	0.914	1.074	1.231	1.226	1.265	1.268	1.268	1.207	1.096	1.022	0.983
	40	0.736	0.768	0.822	0.941	1.022	1.126	1.313	1.307	1.396	1.392	1.354	1.272	1.168	1.096	1.027

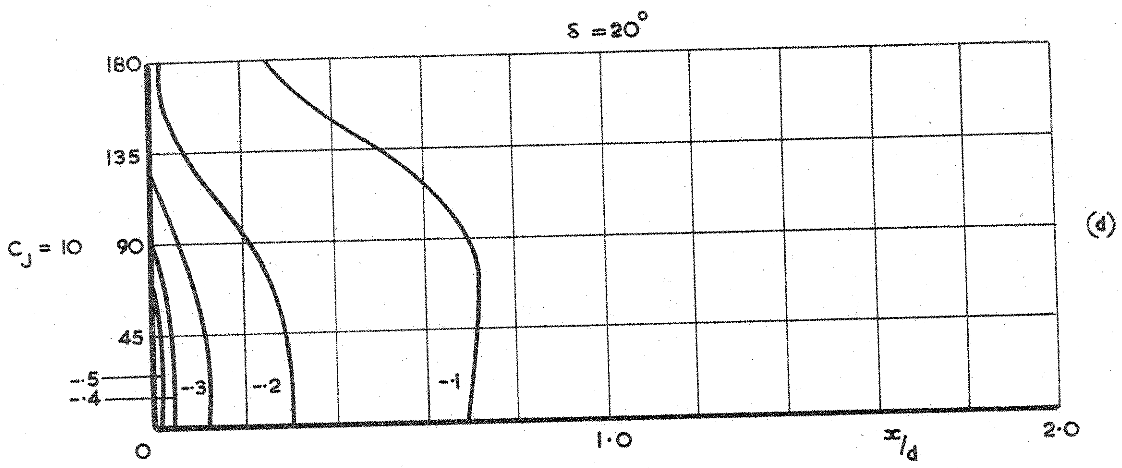

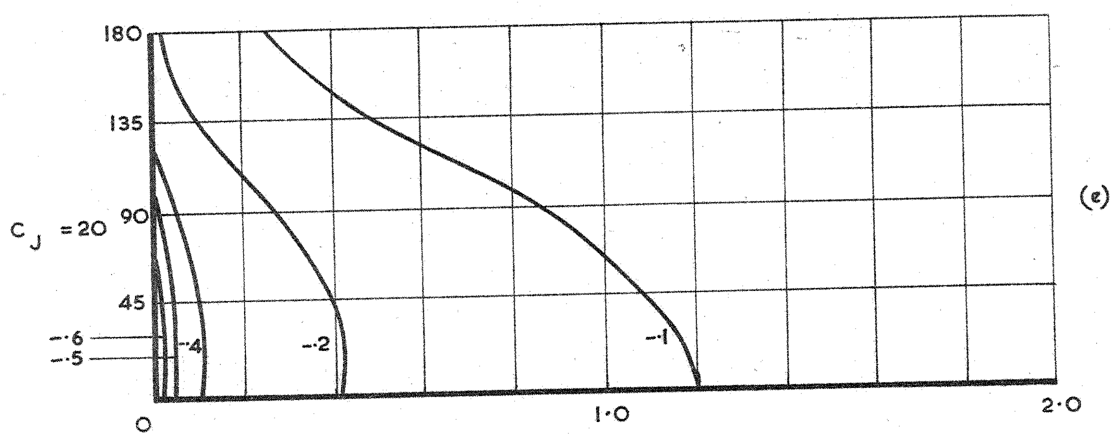

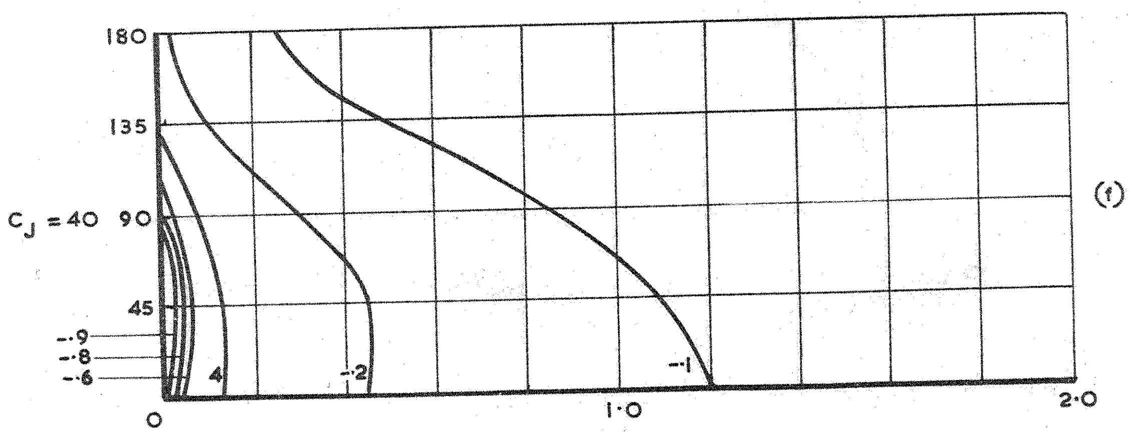

FIG. 5. SIDE PRESSURE DISTRIBUTIONS

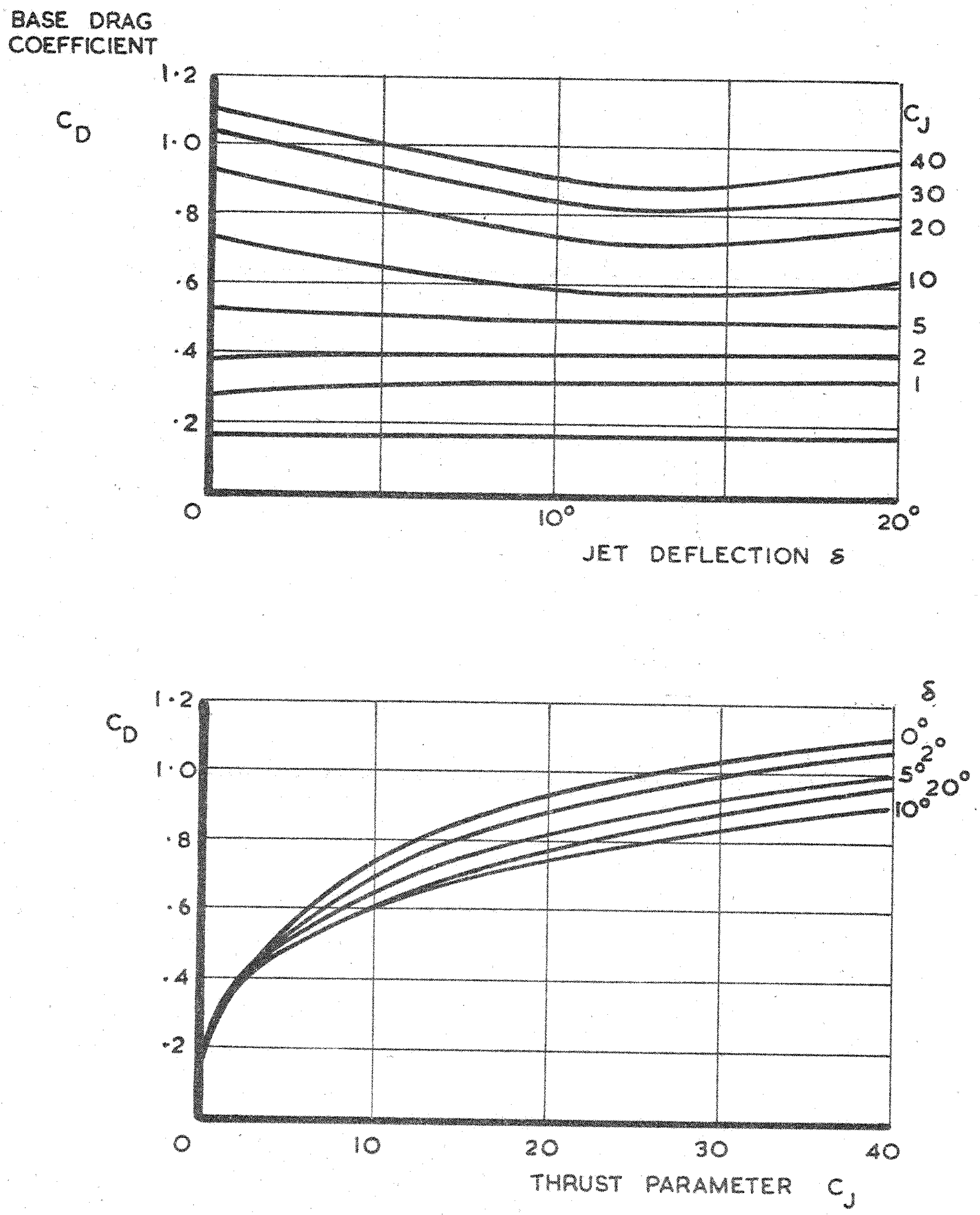

FIG. 6. VARIATION OF BASE DRAG WITH JET DEFLECTION & THRUST

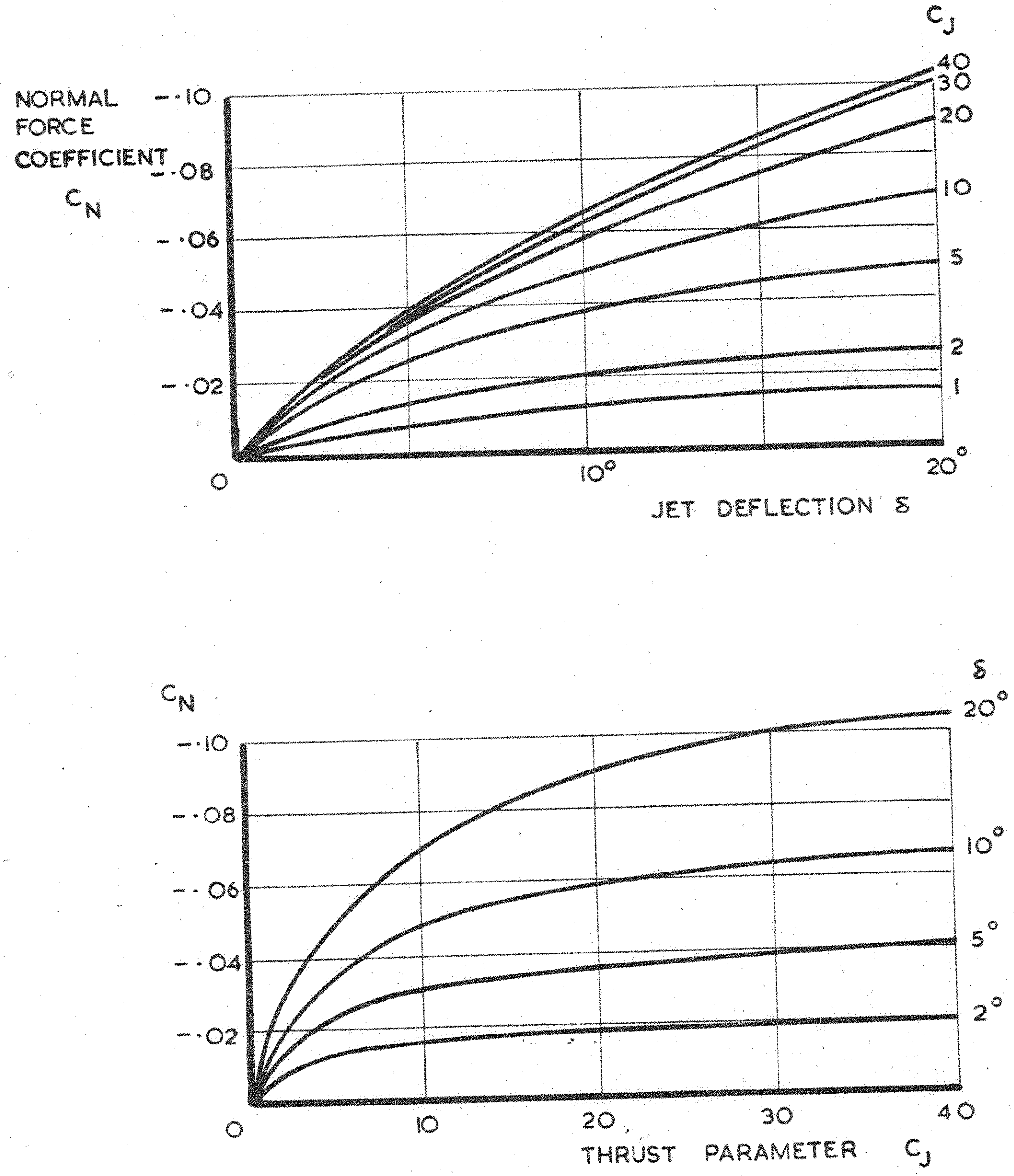

FIG. 7. VARIATION OF SIDE FORCE WITH JET DEFLECTION & THRUST

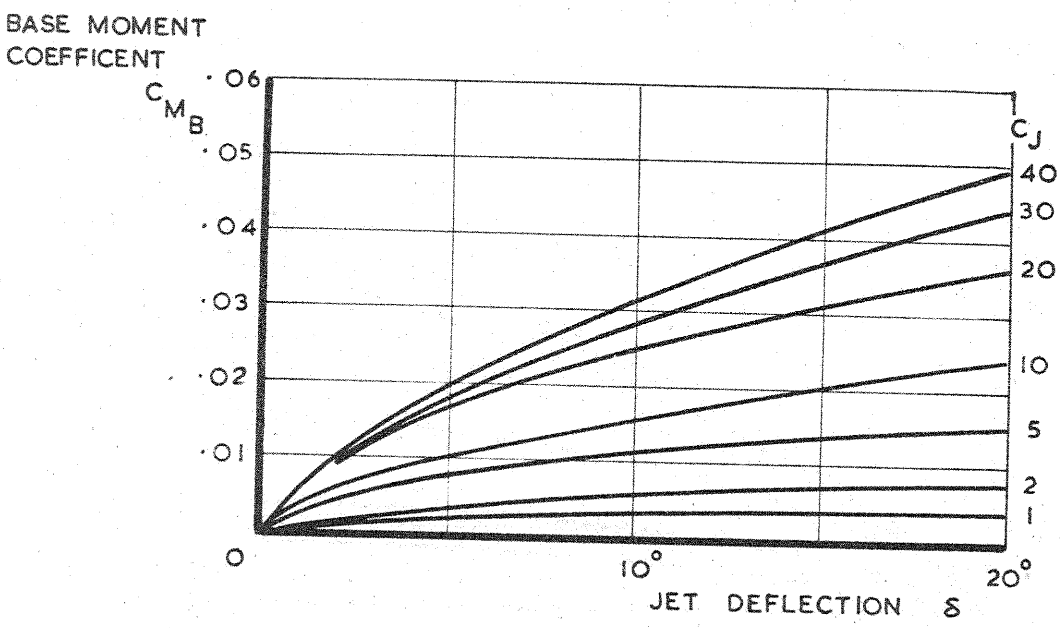

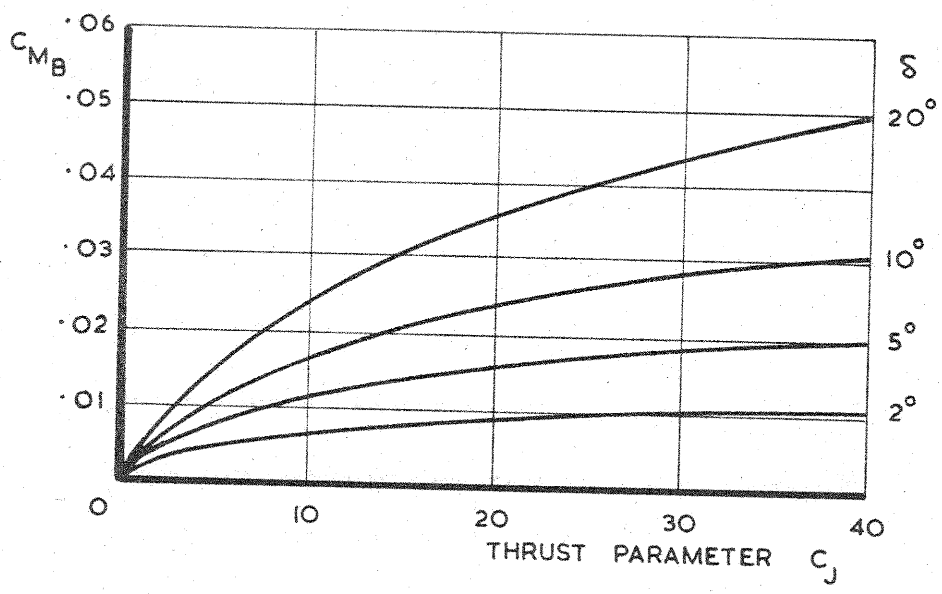

FIG. 8. VARIATION OF BASE MOMENT WITH JET DEFLECTION AND THRUST

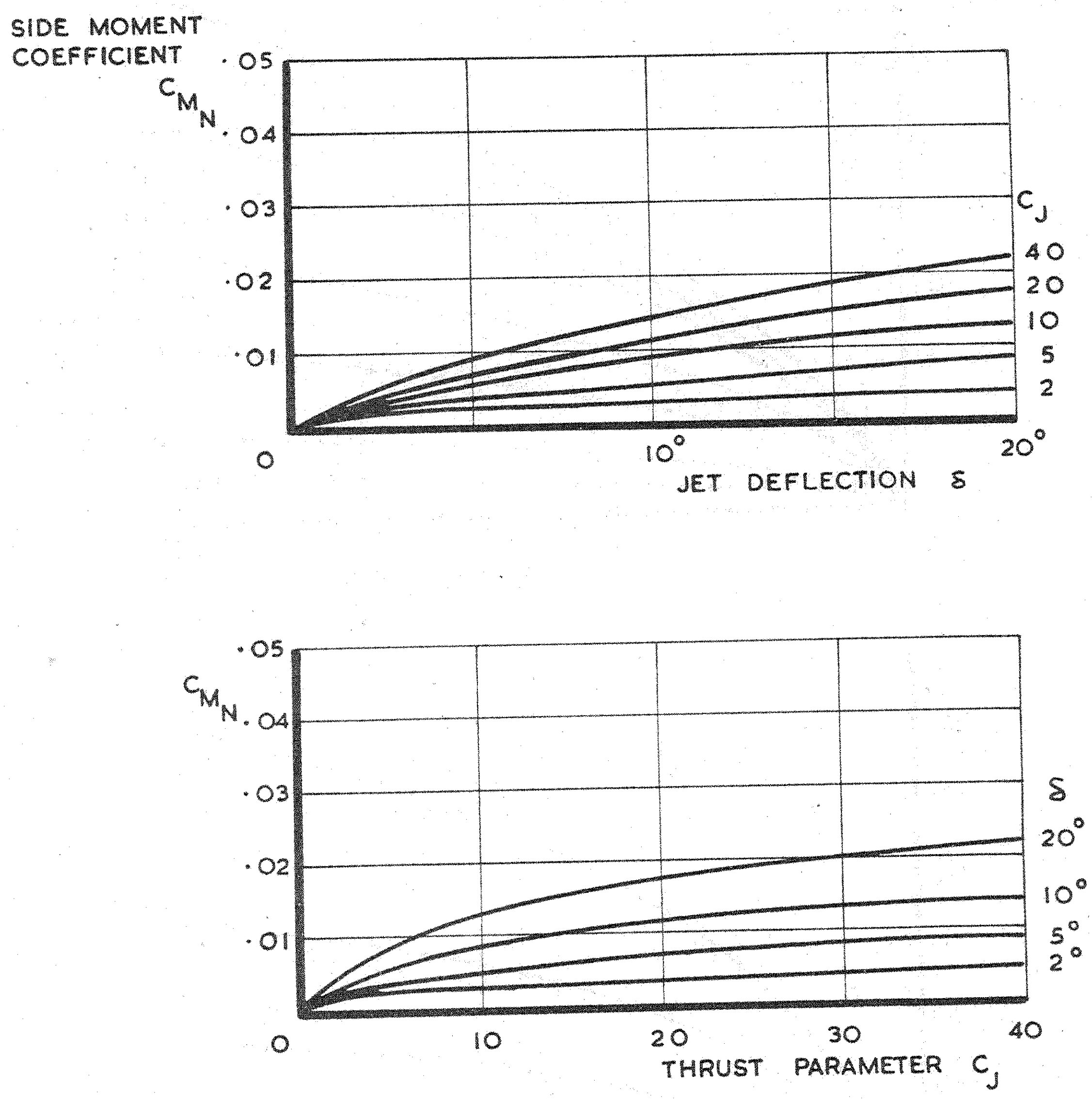

FIG. 9. VARIATION OF SIDE MOMENT WITH JET DEFLECTION AND THRUST

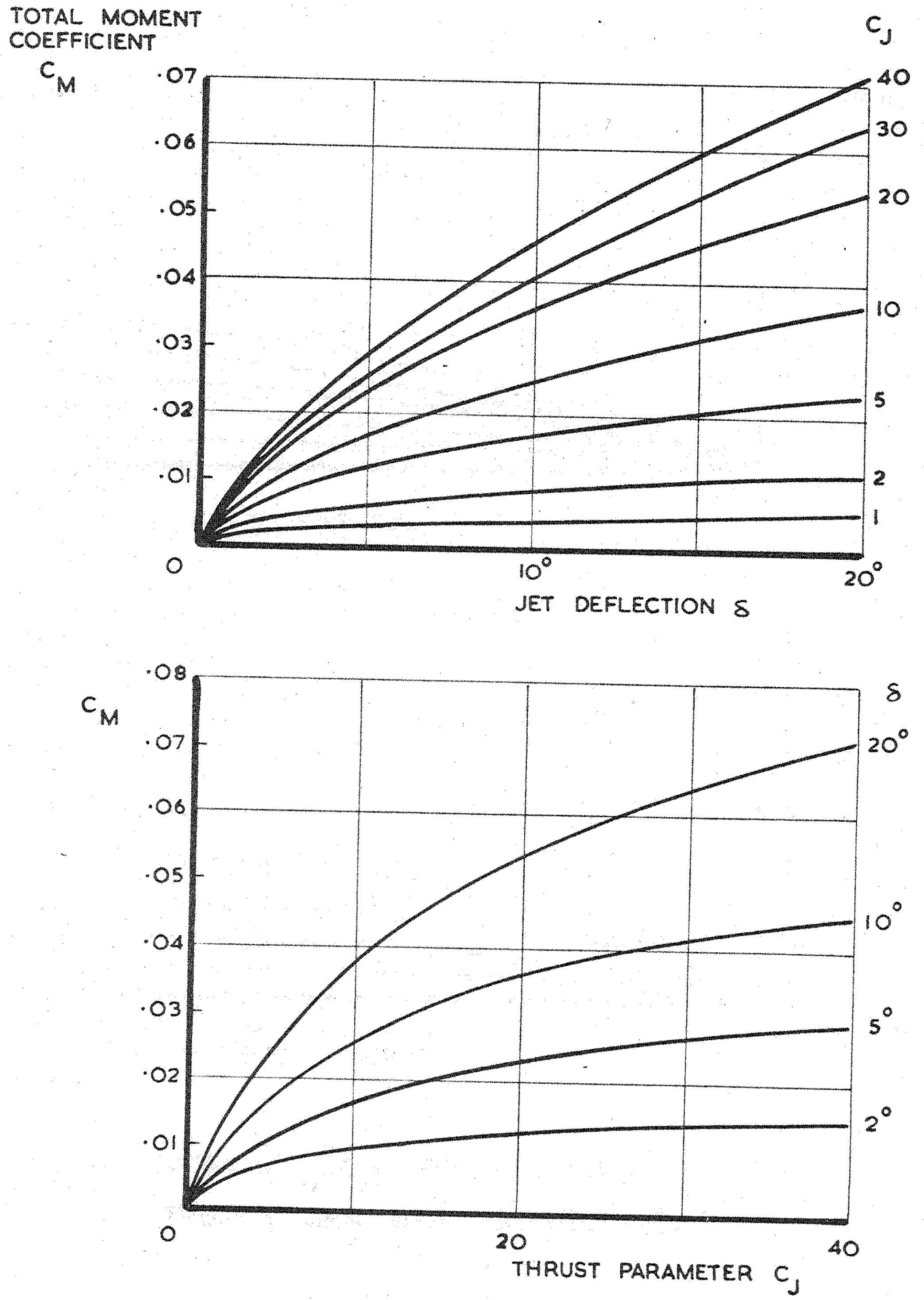

FIG 10. VARIATION OF TOTAL MOMENT WITH JET DEFLECTION AND THRUST

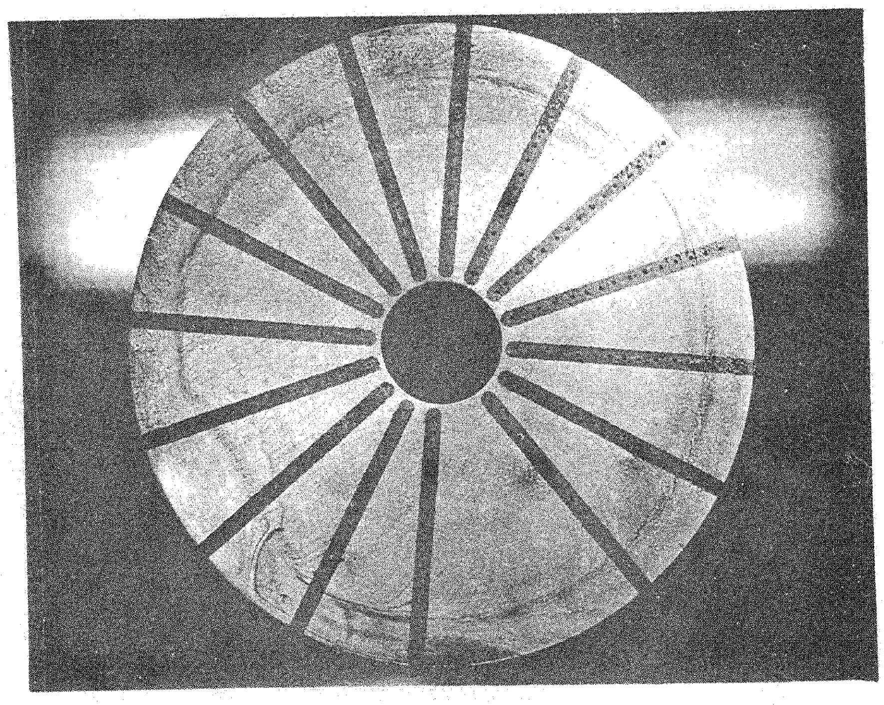

FIG. 11. BASE FLOW PATTERN $C_j = 10$, $\delta = 10^\circ$

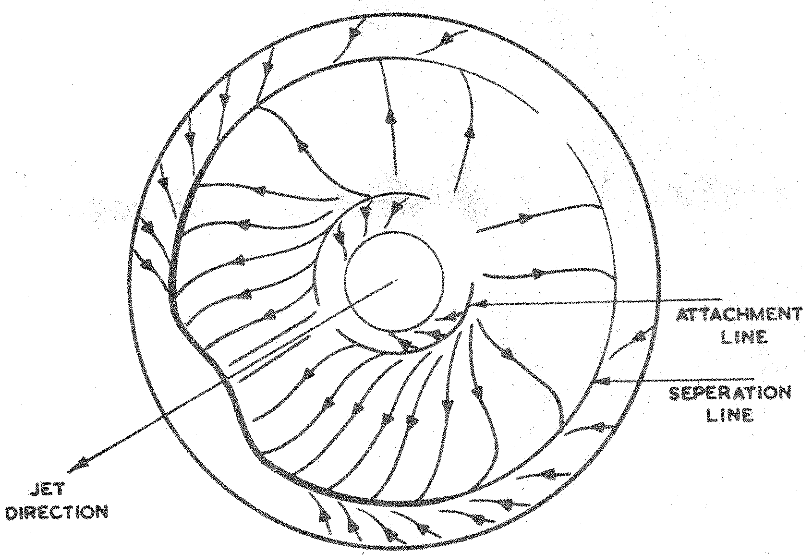

FIG. 12. BASE FLOW DETAILS

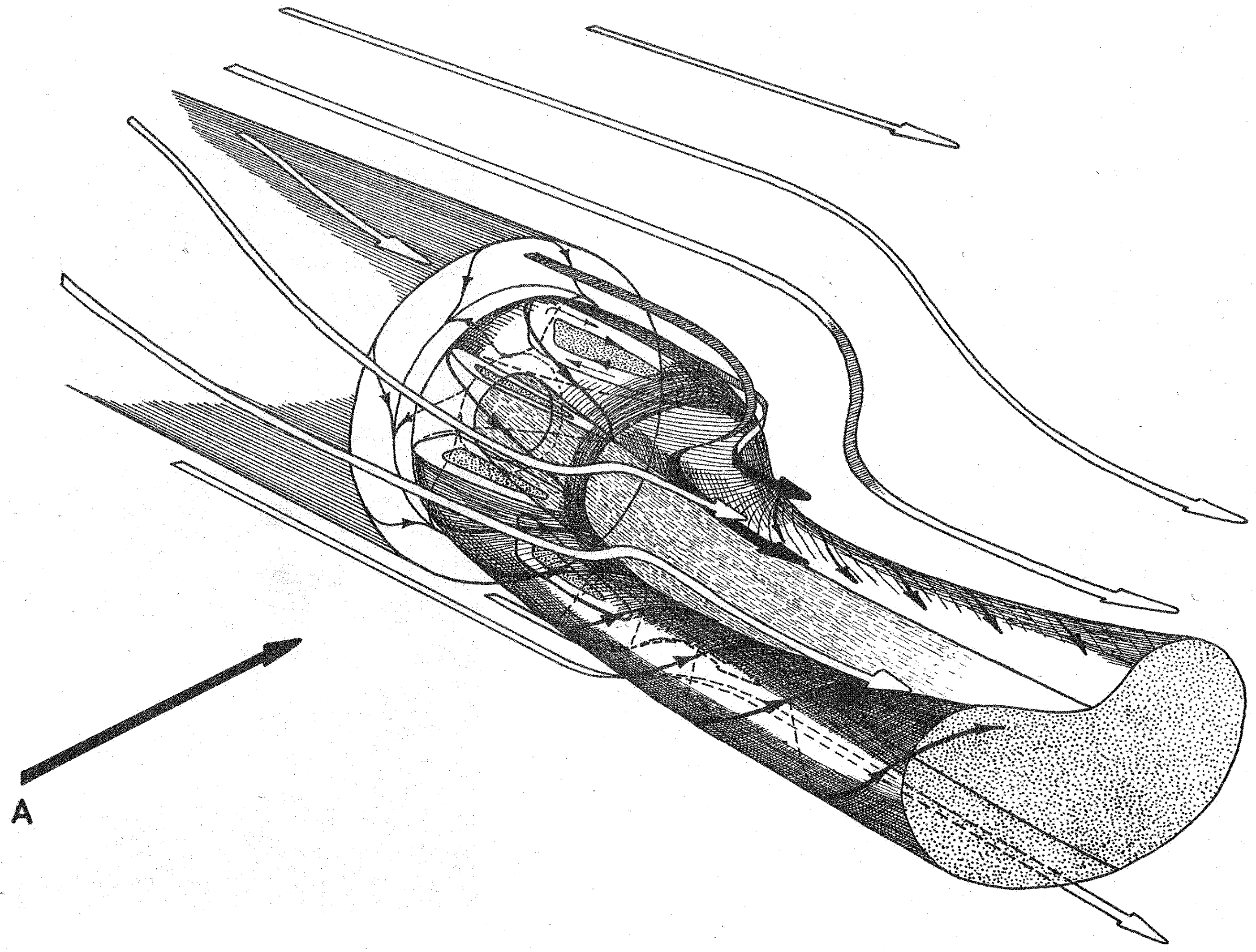

FIG. 13. PICTORIAL VIEW OF FLOW IN MIXING REGION.

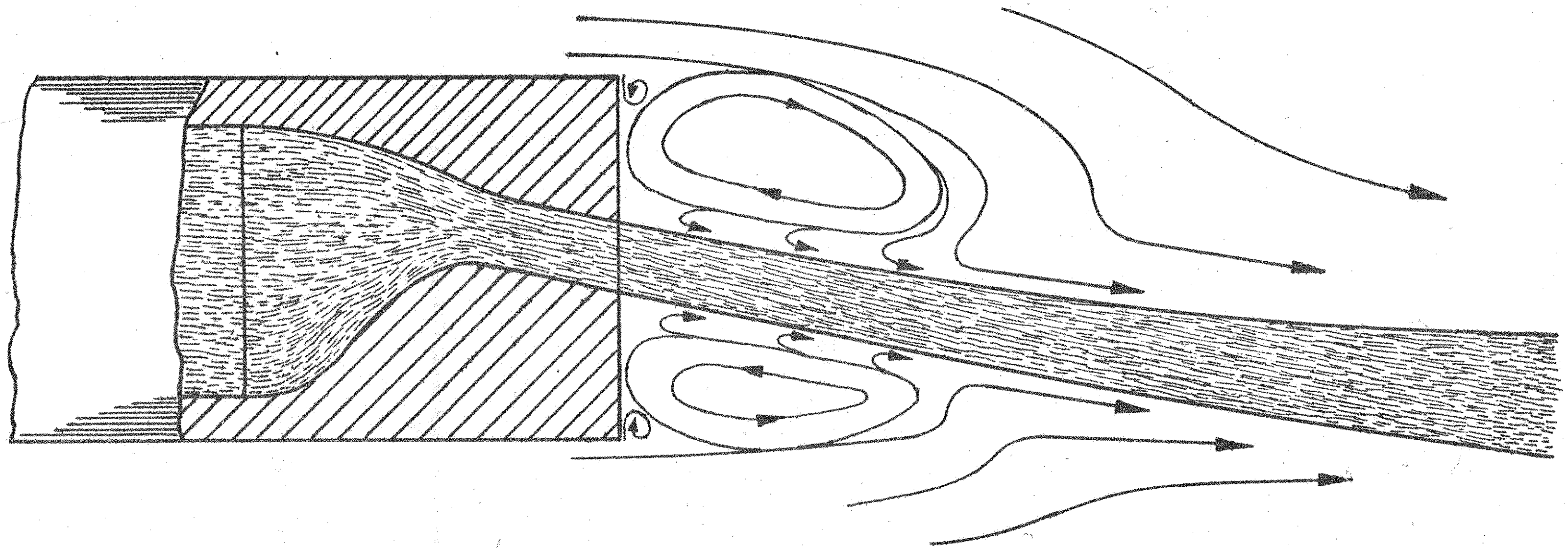

FIG 13a. VIEW IN DIRECTION OF ARROW 'A' AT PLANE OF SYMMETRY.

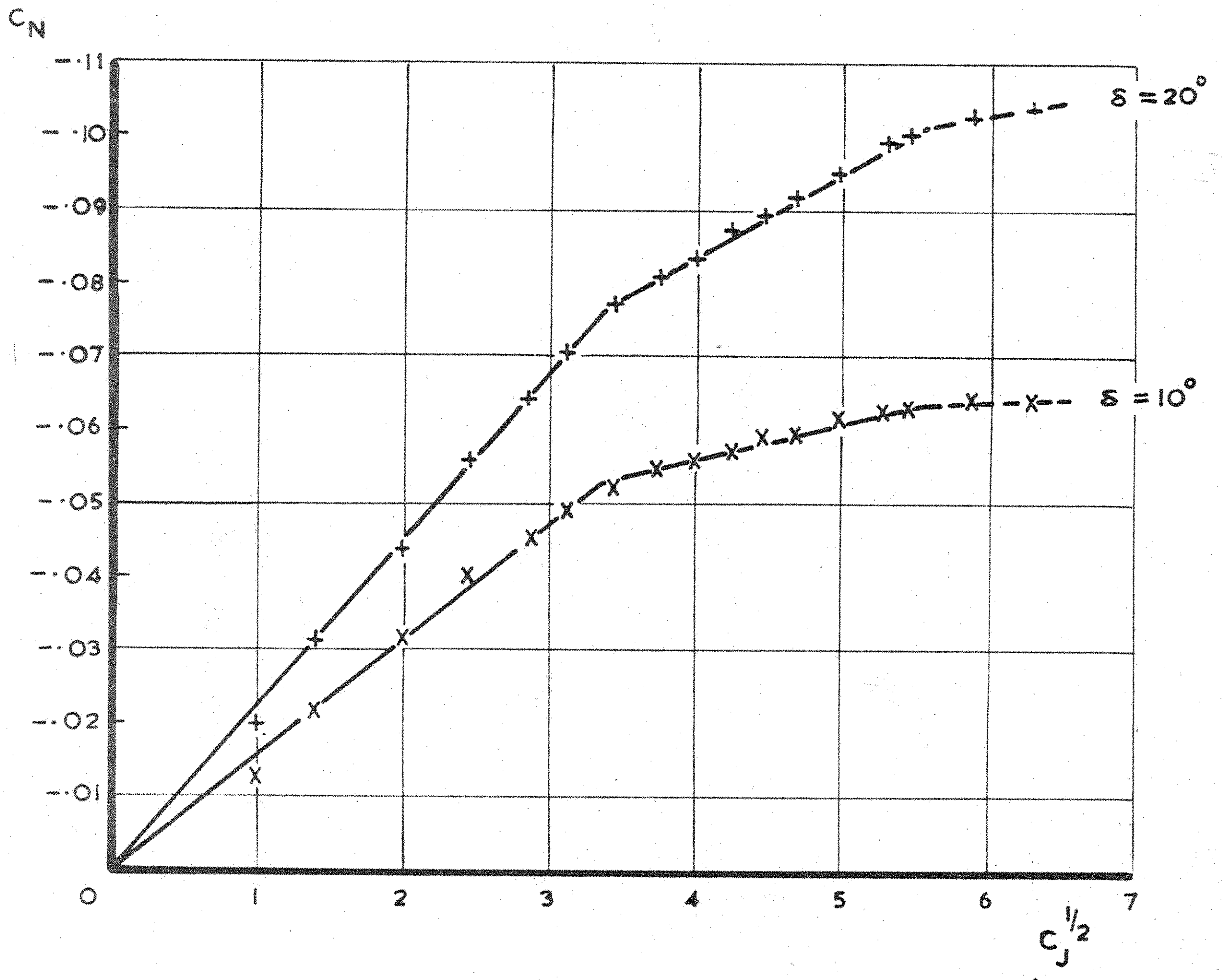

FIG. 14. DEPENDENCE OF SIDE FORCE ON $C_J^{1/2}$

TABLE III. Base Suction Coefficients for 10° jet deflection

	C_J \ $\frac{r}{R}$	0.237	0.287	0.337	0.387	0.437	0.487	0.537	0.587	0.637	0.687	0.737	0.787	0.837	0.887	0.937
$\theta = 0°$	0	0.163	0.163	0.161	0.163	0.165	0.165	0.165	0.165	0.167	0.165	0.167	0.165	0.165	0.165	0.165
	1	0.281	0.302	0.320	0.320	0.322	0.345	0.350	0.360	0.369	0.378	0.376	0.370	0.362	0.361	0.356
	2	0.352	0.354	0.376	0.401	0.438	0.450	0.464	0.478	0.482	0.498	0.490	0.479	0.456	0.441	0.430
	4	0.408	0.410	0.423	0.441	0.462	0.489	0.508	0.529	0.549	0.546	0.553	0.551	0.538	0.522	0.497
	6	0.451	0.453	0.460	0.473	0.502	0.542	0.586	0.633	0.637	0.624	0.672	0.668	0.642	0.609	0.571
	8	0.477	0.480	0.490	0.530	0.567	0.611	0.662	0.702	0.682	0.700	0.724	0.720	0.689	0.654	0.619
	10	0.516	0.522	0.537	0.578	0.637	0.680	0.731	0.804	0.806	0.782	0.817	0.790	0.752	0.703	0.668
	15	0.535	0.542	0.561	0.608	0.660	0.709	0.772	0.835	0.829	0.836	0.865	0.882	0.861	0.826	0.750
	20	0.562	0.564	0.602	0.660	0.709	0.762	0.823	0.870	0.881	0.910	0.941	0.947	0.933	0.900	0.842
	25	0.602	0.625	0.661	0.710	0.761	0.820	0.884	0.932	0.939	0.959	1.000	1.002	0.990	0.951	0.890
	30	0.640	0.642	0.705	0.753	0.810	0.878	0.920	0.981	0.990	1.000	1.039	1.047	1.038	1.002	0.951
	35	0.652	0.655	0.721	0.791	0.841	0.913	0.964	1.007	1.009	1.023	1.072	1.081	1.062	1.020	0.973
	40	0.693	0.688	0.721	0.800	0.871	0.937	0.985	1.040	1.060	1.061	1.096	1.096	1.081	1.037	0.988
$\theta = 22\frac{1}{2}°$	0	0.163	0.165	0.165	0.168	0.165	0.165	0.165	0.165	0.165	0.165	0.165	0.165	0.165	0.165	0.165
	1	0.298	0.321	0.321	0.326	0.330	0.342	0.356	0.362	0.369	0.384	0.384	0.373	0.362	0.362	0.356
	2	0.354	0.362	0.370	0.385	0.401	0.430	0.467	0.483	0.482	0.493	0.487	0.465	0.457	0.442	0.435
	4	0.410	0.410	0.417	0.444	0.478	0.508	0.529	0.553	0.553	0.559	0.573	0.538	0.530	0.518	0.500
	6	0.452	0.452	0.458	0.473	0.518	0.571	0.605	0.651	0.649	0.656	0.681	0.668	0.634	0.602	0.565
	8	0.477	0.477	0.482	0.532	0.567	0.626	0.682	0.714	0.688	0.711	0.724	0.707	0.675	0.644	0.619
	10	0.502	0.502	0.530	0.575	0.624	0.680	0.736	0.782	0.786	0.794	0.791	0.767	0.731	0.686	0.651
	15	0.535	0.535	0.544	0.606	0.652	0.710	0.769	0.829	0.846	0.846	0.898	0.882	0.847	0.800	0.736
	20	0.564	0.560	0.596	0.641	0.695	0.762	0.823	0.882	0.910	0.942	0.960	0.940	0.907	0.860	0.823
	25	0.586	0.592	0.632	0.696	0.746	0.806	0.880	0.937	0.962	0.998	1.016	1.000	0.966	0.902	0.858
	30	0.620	0.622	0.641	0.738	0.791	0.868	0.926	0.990	1.024	1.042	1.064	1.047	1.020	0.965	0.911
	35	0.642	0.645	0.693	0.768	0.826	0.893	0.964	1.024	1.064	1.064	1.102	1.102	1.038	0.993	0.932
	40	0.661	0.661	0.714	0.782	0.856	0.922	0.990	1.040	1.096	1.127	1.142	1.127	1.066	1.064	0.955
$\theta = 45°$	0	0.165	0.165	0.166	0.165	0.165	0.163	0.165	0.165	0.165	0.167	0.165	0.165	0.165	0.165	0.165
	1	0.329	0.323	0.325	0.329	0.338	0.344	0.358	0.367	0.363	0.396	0.381	0.366	0.362	0.358	0.355
	2	0.361	0.360	0.369	0.385	0.404	0.418	0.463	0.486	0.482	0.504	0.483	0.469	0.457	0.442	0.439
	4	0.410	0.411	0.417	0.444	0.486	0.522	0.550	0.568	0.568	0.591	0.559	0.532	0.518	0.507	0.500
	6	0.452	0.452	0.458	0.481	0.532	0.594	0.628	0.671	0.662	0.688	0.688	0.657	0.620	0.593	0.576
	8	0.477	0.477	0.482	0.521	0.570	0.642	0.689	0.721	0.711	0.723	0.722	0.698	0.660	0.631	0.610
	10	0.495	0.499	0.528	0.565	0.610	0.675	0.738	0.770	0.782	0.804	0.791	0.752	0.711	0.672	0.648
	15	0.537	0.536	0.550	0.606	0.652	0.710	0.767	0.822	0.860	0.858	0.922	0.878	0.823	0.780	0.736
	20	0.552	0.557	0.581	0.637	0.692	0.758	0.822	0.896	0.957	0.976	0.978	0.939	0.882	0.829	0.779
	25	0.571	0.578	0.619	0.680	0.731	0.797	0.878	0.942	0.999	1.034	1.022	0.991	0.935	0.880	0.842
	30	0.603	0.611	0.648	0.717	0.782	0.859	0.926	0.997	1.054	1.096	1.104	1.070	0.999	0.922	0.860
	35	0.620	0.629	0.676	0.741	0.804	0.882	0.961	1.031	1.092	1.139	1.158	1.120	1.032	0.958	0.880
	40	0.632	0.651	0.698	0.766	0.831	0.903	0.990	1.064	1.127	1.182	1.194	1.158	1.066	0.974	0.893

TABLE III. (Cont) Base Suction Coefficients for 10° jet deflection

θ	C_J \ $\frac{r}{R}$	0.237	0.287	0.337	0.387	0.437	0.487	0.537	0.587	0.637	0.687	0.737	0.787	0.837	0.887	0.937
$\theta = 67\frac{1}{2}^{\circ}$																
	0	0.163	0.165	0.165	0.165	0.165	0.165	0.165	0.165	0.165	0.165	0.165	0.165	0.163	0.165	0.165
	1	0.321	0.321	0.321	0.329	0.336	0.342	0.347	0.363	0.363	0.372	0.372	0.354	0.342	0.342	0.339
	2	0.346	0.344	0.354	0.376	0.404	0.404	0.456	0.464	0.479	0.486	0.480	0.444	0.426	0.426	0.404
	4	0.385	0.385	0.396	0.426	0.452	0.486	0.527	0.550	0.548	0.568	0.547	0.518	0.500	0.479	0.456
	6	0.404	0.407	0.411	0.444	0.486	0.532	0.574	0.636	0.628	0.642	0.661	0.620	0.568	0.539	0.502
	8	0.413	0.411	0.426	0.483	0.527	0.583	0.628	0.681	0.671	0.688	0.680	0.657	0.593	0.582	0.562
	10	0.448	0.446	0.452	0.504	0.553	0.613	0.673	0.721	0.736	0.744	0.732	0.711	0.664	0.628	0.581
	15	0.477	0.475	0.490	0.546	0.605	0.656	0.738	0.800	0.843	0.835	0.886	0.835	0.786	0.721	0.657
	20	0.495	0.492	0.521	0.587	0.642	0.710	0.782	0.858	0.910	0.937	0.942	0.912	0.867	0.776	0.703
	25	0.502	0.502	0.550	0.606	0.673	0.736	0.824	0.896	0.959	0.998	0.995	0.978	0.896	0.821	0.736
	30	0.518	0.524	0.571	0.638	0.707	0.782	0.858	0.942	0.991	1.039	1.048	1.032	0.939	0.854	0.779
	35	0.532	0.536	0.587	0.656	0.712	0.800	0.886	0.962	1.024	1.068	1.070	1.064	0.976	0.878	0.798
	40	0.547	0.549	0.602	0.665	0.738	0.817	0.898	0.986	1.047	1.102	1.102	1.082	1.000	0.906	0.812
$\theta = 90^{\circ}$																
	0	0.166	0.165	0.165	0.165	0.167	0.166	0.166	0.165	0.163	0.163	0.165	0.165	0.165	0.165	0.165
	1	0.321	0.321	0.323	0.329	0.336	0.339	0.347	0.360	0.349	0.368	0.365	0.349	0.342	0.336	0.322
	2	0.332	0.335	0.341	0.362	0.391	0.402	0.442	0.457	0.463	0.461	0.479	0.440	0.418	0.399	0.389
	4	0.356	0.354	0.362	0.383	0.417	0.448	0.491	0.532	0.527	0.546	0.544	0.502	0.471	0.442	0.421
	6	0.364	0.363	0.370	0.400	0.438	0.487	0.539	0.601	0.586	0.581	0.623	0.561	0.523	0.484	0.446
	8	0.375	0.378	0.381	0.424	0.476	0.518	0.573	0.636	0.642	0.645	0.641	0.602	0.560	0.523	0.478
	10	0.394	0.400	0.411	0.449	0.491	0.542	0.618	0.680	0.683	0.671	0.682	0.669	0.628	0.581	0.527
	15	0.410	0.411	0.433	0.478	0.542	0.593	0.691	0.775	0.832	0.810	0.843	0.803	0.749	0.675	0.582
	20	0.439	0.442	0.465	0.521	0.583	0.661	0.747	0.822	0.873	0.902	0.910	0.890	0.821	0.722	0.638
	25	0.442	0.445	0.482	0.540	0.610	0.694	0.778	0.845	0.907	0.963	0.968	0.961	0.864	0.768	0.662
	30	0.447	0.453	0.498	0.552	0.622	0.711	0.796	0.880	0.941	0.989	1.006	0.992	0.901	0.800	0.698
	35	0.453	0.462	0.503	0.559	0.638	0.730	0.821	0.902	0.962	1.004	1.021	1.009	0.923	0.819	0.713
	40	0.459	0.478	0.512	0.563	0.643	0.742	0.842	0.923	0.991	1.022	1.039	1.018	0.942	0.840	0.722
$\theta = 112\frac{1}{2}^{\circ}$																
	0	0.165	0.165	0.165	0.165	0.163	0.165	0.163	0.165	0.165	0.167	0.165	0.165	0.165	0.165	0.165
	1	0.306	0.306	0.306	0.309	0.316	0.323	0.329	0.337	0.332	0.347	0.344	0.333	0.329	0.321	0.306
	2	0.312	0.316	0.318	0.329	0.354	0.366	0.391	0.411	0.421	0.428	0.439	0.418	0.391	0.363	0.348
	4	0.310	0.306	0.329	0.356	0.367	0.404	0.438	0.462	0.462	0.489	0.486	0.464	0.436	0.411	0.376
	6	0.310	0.310	0.326	0.352	0.381	0.438	0.479	0.539	0.502	0.544	0.561	0.513	0.479	0.444	0.398
	8	0.316	0.318	0.320	0.356	0.402	0.463	0.518	0.566	0.581	0.605	0.600	0.566	0.526	0.468	0.421
	10	0.314	0.318	0.324	0.367	0.421	0.479	0.546	0.611	0.645	0.636	0.636	0.627	0.581	0.526	0.464
	15	0.314	0.318	0.337	0.381	0.453	0.515	0.602	0.674	0.726	0.738	0.742	0.738	0.665	0.592	0.508
	20	0.323	0.320	0.358	0.406	0.479	0.562	0.656	0.723	0.783	0.817	0.803	0.785	0.711	0.643	0.554
	25	0.329	0.327	0.358	0.412	0.498	0.587	0.672	0.738	0.800	0.826	0.832	0.835	0.756	0.671	0.564
	30	0.326	0.326	0.365	0.418	0.502	0.585	0.681	0.765	0.822	0.861	0.865	0.858	0.787	0.689	0.584
	35	0.332	0.335	0.368	0.418	0.507	0.594	0.707	0.798	0.837	0.872	0.875	0.863	0.792	0.707	0.598
	40	0.332	0.330	0.374	0.421	0.516	0.611	0.707	0.810	0.856	0.884	0.882	0.863	0.800	0.711	0.611

TABLE III. (Cont) Base Suction Coefficients for 10° jet deflection

	C_J \ $\frac{r}{R}$	0.237	0.287	0.337	0.387	0.437	0.487	0.537	0.587	0.637	0.687	0.737	0.787	0.837	0.887	0.937
$\theta = 135^{\circ}$	0	0.165	0.165	0.165	0.163	0.165	0.165	0.165	0.167	0.165	0.165	0.165	0.165	0.165	0.165	0.165
	1	0.298	0.296	0.296	0.298	0.300	0.306	0.309	0.318	0.316	0.322	0.324	0.320	0.311	0.300	0.288
	2	0.296	0.296	0.296	0.298	0.306	0.323	0.342	0.364	0.382	0.396	0.399	0.396	0.369	0.342	0.316
	4	0.271	0.272	0.280	0.296	0.321	0.352	0.375	0.391	0.412	0.429	0.440	0.416	0.384	0.357	0.331
	6	0.260	0.258	0.271	0.290	0.330	0.374	0.418	0.467	0.448	0.487	0.506	0.479	0.428	0.388	0.348
	8	0.247	0.250	0.260	0.288	0.342	0.398	0.451	0.509	0.537	0.553	0.553	0.532	0.482	0.424	0.372
	10	0.222	0.227	0.239	0.285	0.350	0.421	0.490	0.552	0.589	0.602	0.597	0.573	0.541	0.478	0.399
	15	0.220	0.223	0.230	0.285	0.358	0.439	0.518	0.591	0.656	0.646	0.671	0.690	0.609	0.520	0.442
	20	0.217	0.220	0.230	0.285	0.361	0.467	0.556	0.629	0.688	0.717	0.729	0.709	0.644	0.561	0.474
	25	0.214	0.218	0.230	0.285	0.361	0.470	0.562	0.637	0.696	0.730	0.733	0.717	0.655	0.574	0.485
	30	0.213	0.213	0.230	0.285	0.367	0.474	0.566	0.648	0.703	0.742	0.748	0.721	0.660	0.581	0.492
	35	0.210	0.213	0.230	0.285	0.372	0.482	0.571	0.656	0.715	0.753	0.753	0.728	0.672	0.586	0.499
	40	0.208	0.213	0.230	0.285	0.378	0.482	0.577	0.663	0.722	0.767	0.761	0.732	0.678	0.592	0.503
$\theta = 157\frac{1}{2}^{\circ}$	0	0.165	0.165	0.165	0.165	0.165	0.163	0.165	0.165	0.165	0.163	0.165	0.165	0.165	0.165	0.165
	1	0.254	0.256	0.256	0.264	0.268	0.275	0.284	0.289	0.289	0.292	0.292	0.286	0.286	0.277	0.269
	2	0.263	0.263	0.258	0.258	0.262	0.279	0.318	0.322	0.328	0.336	0.334	0.327	0.327	0.318	0.300
	4	0.163	0.257	0.252	0.259	0.267	0.289	0.327	0.342	0.349	0.357	0.357	0.354	0.334	0.331	0.314
	6	0.241	0.232	0.228	0.247	0.267	0.306	0.356	0.413	0.416	0.439	0.449	0.447	0.400	0.366	0.318
	8	0.217	0.215	0.215	0.233	0.267	0.337	0.406	0.454	0.464	0.487	0.516	0.502	0.467	0.402	0.337
	10	0.190	0.190	0.194	0.216	0.254	0.358	0.443	0.498	0.521	0.562	0.569	0.551	0.503	0.431	0.353
	15	0.186	0.183	0.186	0.221	0.258	0.381	0.465	0.537	0.596	0.624	0.656	0.643	0.572	0.503	0.416
	20	0.182	0.178	0.180	0.238	0.306	0.402	0.490	0.566	0.635	0.676	0.689	0.671	0.613	0.530	0.447
	25	0.178	0.178	0.184	0.238	0.306	0.411	0.501	0.573	0.651	0.683	0.702	0.682	0.619	0.537	0.447
	30	0.176	0.172	0.180	0.238	0.302	0.416	0.508	0.589	0.656	0.695	0.702	0.686	0.623	0.544	0.452
	35	0.165	0.172	0.176	0.238	0.300	0.416	0.508	0.593	0.665	0.702	0.708	0.686	0.626	0.540	0.465
	40	0.168	0.172	0.176	0.238	0.300	0.418	0.512	0.602	0.669	0.713	0.715	0.688	0.630	0.552	0.479
$\theta = 180^{\circ}$	0	0.165	0.163	0.165	0.165	0.163	0.165	0.165	0.165	0.165	0.165	0.165	0.165	0.167	0.165	0.165
	1	0.247	0.241	0.250	0.253	0.256	0.256	0.264	0.271	0.271	0.279	0.279	0.277	0.277	0.271	0.262
	2	0.230	0.232	0.228	0.237	0.243	0.268	0.290	0.300	0.307	0.321	0.318	0.322	0.312	0.300	0.281
	4	0.212	0.212	0.214	0.222	0.243	0.278	0.298	0.312	0.319	0.330	0.330	0.322	0.312	0.286	0.281
	6	0.194	0.192	0.198	0.210	0.243	0.302	0.337	0.378	0.397	0.427	0.447	0.436	0.380	0.352	0.300
	8	0.178	0.180	0.187	0.203	0.243	0.318	0.375	0.424	0.452	0.483	0.502	0.480	0.432	0.371	0.322
	10	0.160	0.162	0.169	0.191	0.243	0.330	0.412	0.473	0.516	0.548	0.532	0.525	0.473	0.401	0.338
	15	0.146	0.144	0.153	0.188	0.247	0.351	0.440	0.502	0.563	0.616	0.648	0.628	0.559	0.492	0.386
	20	0.140	0.140	0.150	0.188	0.247	0.351	0.444	0.530	0.595	0.647	0.681	0.642	0.580	0.502	0.410
	25	0.134	0.138	0.146	0.185	0.247	0.351	0.451	0.543	0.606	0.656	0.681	0.640	0.580	0.502	0.412
	30	0.130	0.134	0.140	0.181	0.250	0.356	0.458	0.550	0.612	0.665	0.681	0.640	0.580	0.506	0.424
	35	0.128	0.134	0.137	0.181	0.250	0.356	0.458	0.568	0.635	0.675	0.684	0.637	0.580	0.510	0.444
	40	0.128	0.130	0.137	0.181	0.258	0.356	0.462	0.573	0.635	0.682	0.684	0.637	0.580	0.512	0.449

TABLE IV. Base Suction Coefficients for 20° jet deflection

θ	C_J \ $\frac{r}{R}$	0.237	0.287	0.337	0.387	0.437	0.487	0.537	0.587	0.637	0.687	0.737	0.787	0.837	0.887	0.937
$\theta = 0°$																
	0	0.165	0.165	0.165	0.163	0.165	0.165	0.167	0.165	0.165	0.163	0.165	0.165	0.165	0.165	0.165
	1	0.372	0.346	0.340	0.351	0.362	0.370	0.378	0.360	0.379	0.379	0.376	0.366	0.350	0.359	0.356
	2	0.448	0.430	0.430	0.438	0.440	0.444	0.459	0.462	0.471	0.468	0.468	0.461	0.463	0.459	0.459
	4	0.533	0.509	0.509	0.511	0.518	0.528	0.528	0.541	0.548	0.549	0.541	0.533	0.519	0.521	0.517
	6	0.579	0.561	0.555	0.568	0.568	0.586	0.606	0.608	0.622	0.626	0.633	0.628	0.619	0.600	0.582
	8	0.622	0.603	0.589	0.599	0.603	0.624	0.647	0.680	0.716	0.707	0.717	0.709	0.718	0.692	0.653
	10	0.676	0.657	0.657	0.678	0.698	0.718	0.738	0.762	0.788	0.806	0.820	0.826	0.829	0.781	0.709
	15	0.729	0.700	0.693	0.698	0.710	0.729	0.752	0.779	0.810	0.850	0.869	0.900	0.896	0.852	0.791
	20	0.734	0.718	0.710	0.712	0.722	0.748	0.777	0.811	0.868	0.913	0.958	0.982	0.980	0.956	0.872
	25	0.748	0.722	0.718	0.718	0.724	0.756	0.801	0.852	0.921	0.986	1.015	1.042	1.039	1.007	0.940
	30	0.756	0.731	0.722	0.724	0.738	0.770	0.831	0.901	0.963	1.032	1.086	1.100	1.096	1.071	1.002
	35	0.762	0.742	0.728	0.734	0.750	0.801	0.861	0.929	1.011	1.060	1.115	1.136	1.128	1.096	1.038
	40	0.771	0.752	0.737	0.737	0.769	0.812	0.898	0.972	1.047	1.123	1.169	1.187	1.176	1.140	1.073
$\theta = 22\frac{1}{2}°$																
	0	0.165	0.165	0.165	0.165	0.165	0.163	0.165	0.165	0.165	0.165	0.165	0.167	0.165	0.165	0.165
	1	0.366	0.346	0.346	0.351	0.362	0.370	0.378	0.372	0.376	0.379	0.368	0.366	0.352	0.352	0.352
	2	0.438	0.423	0.423	0.430	0.440	0.444	0.462	0.462	0.472	0.472	0.468	0.460	0.456	0.452	0.448
	4	0.526	0.500	0.496	0.506	0.498	0.507	0.523	0.538	0.546	0.546	0.528	0.530	0.516	0.502	0.496
	6	0.567	0.556	0.545	0.562	0.566	0.582	0.612	0.615	0.632	0.617	0.633	0.624	0.613	0.596	0.572
	8	0.613	0.593	0.582	0.596	0.606	0.631	0.650	0.686	0.719	0.712	0.718	0.704	0.702	0.642	0.613
	10	0.670	0.645	0.643	0.666	0.682	0.724	0.742	0.774	0.800	0.814	0.826	0.819	0.803	0.738	0.702
	15	0.713	0.683	0.688	0.687	0.710	0.756	0.806	0.838	0.865	0.902	0.913	0.910	0.886	0.846	0.784
	20	0.730	0.715	0.712	0.710	0.726	0.774	0.825	0.871	0.936	0.973	0.998	1.010	0.980	0.950	0.865
	25	0.746	0.722	0.716	0.716	0.742	0.801	0.854	0.926	0.984	1.047	1.060	1.053	1.036	0.984	0.936
	30	0.752	0.731	0.728	0.728	0.765	0.826	0.902	0.957	1.033	1.096	1.104	1.104	1.090	1.053	0.996
	35	0.762	0.744	0.728	0.746	0.796	0.843	0.948	0.984	1.100	1.136	1.140	1.148	1.122	1.088	1.040
	40	0.771	0.755	0.755	0.754	0.803	0.865	0.996	1.060	1.187	1.257	1.216	1.206	1.178	1.132	1.056
$\theta = 45°$																
	0	0.165	0.165	0.163	0.165	0.165	0.167	0.165	0.163	0.165	0.165	0.165	0.165	0.165	0.165	0.165
	1	0.359	0.350	0.342	0.343	0.358	0.371	0.379	0.376	0.381	0.372	0.363	0.360	0.357	0.341	0.348
	2	0.429	0.418	0.418	0.420	0.433	0.440	0.447	0.461	0.472	0.472	0.462	0.460	0.448	0.442	0.431
	4	0.508	0.486	0.474	0.480	0.486	0.498	0.509	0.521	0.533	0.539	0.526	0.521	0.508	0.491	0.473
	6	0.552	0.531	0.528	0.542	0.559	0.581	0.606	0.627	0.635	0.629	0.625	0.613	0.598	0.569	0.548
	8	0.595	0.577	0.570	0.582	0.609	0.631	0.660	0.701	0.719	0.720	0.718	0.696	0.682	0.646	0.612
	10	0.636	0.619	0.610	0.622	0.659	0.721	0.760	0.802	0.831	0.838	0.838	0.811	0.778	0.742	0.693
	15	0.702	0.672	0.660	0.668	0.709	0.778	0.852	0.928	0.971	0.977	0.980	0.936	0.895	0.842	0.769
	20	0.721	0.702	0.688	0.702	0.753	0.822	0.894	0.988	1.042	1.069	1.058	1.022	0.981	0.928	0.873
	25	0.738	0.719	0.707	0.731	0.783	0.861	0.949	1.020	1.084	1.120	1.106	1.073	1.021	0.973	0.908
	30	0.749	0.736	0.722	0.746	0.822	0.900	0.987	1.072	1.136	1.162	1.144	1.118	1.072	1.011	0.950
	35	0.772	0.750	0.750	0.778	0.857	0.948	1.050	1.141	1.202	1.228	1.202	1.164	1.118	1.072	1.018
	40	0.790	0.764	0.764	0.800	0.896	1.002	1.124	1.242	1.316	1.318	1.287	1.236	1.188	1.140	1.078

TABLE IV. (Cont) Base Suction Coefficients for 20° jet deflection

θ	C_J \ $\frac{r}{R}$	0.237	0.287	0.337	0.387	0.437	0.487	0.537	0.587	0.637	0.687	0.737	0.787	0.837	0.887	0.937
$\theta = 67\frac{1}{2}^{\circ}$	0	0.165	0.165	0.163	0.163	0.163	0.163	0.161	0.165	0.165	0.165	0.165	0.165	0.165	0.165	0.165
	1	0.352	0.346	0.328	0.333	0.346	0.362	0.365	0.365	0.368	0.356	0.351	0.347	0.336	0.330	0.322
	2	0.410	0.402	0.392	0.396	0.410	0.418	0.428	0.428	0.447	0.454	0.444	0.432	0.420	0.414	0.401
	4	0.456	0.446	0.434	0.446	0.458	0.476	0.498	0.494	0.506	0.509	0.502	0.488	0.464	0.451	0.433
	6	0.483	0.485	0.466	0.478	0.527	0.541	0.560	0.582	0.598	0.598	0.590	0.562	0.544	0.522	0.496
	8	0.522	0.516	0.506	0.546	0.564	0.582	0.622	0.668	0.665	0.667	0.656	0.635	0.612	0.570	0.537
	10	0.567	0.556	0.550	0.568	0.616	0.654	0.726	0.734	0.765	0.786	0.772	0.733	0.675	0.654	0.604
	15	0.629	0.604	0.602	0.619	0.696	0.752	0.814	0.879	0.932	0.936	0.936	0.892	0.851	0.769	0.702
	20	0.650	0.638	0.643	0.684	0.746	0.808	0.872	0.950	1.016	1.024	1.016	1.002	0.928	0.852	0.786
	25	0.678	0.652	0.657	0.708	0.768	0.832	0.926	0.996	1.047	1.097	1.064	1.044	0.962	0.894	0.823
	30	0.682	0.670	0.672	0.725	0.804	0.886	0.973	1.056	1.100	1.126	1.104	1.078	1.002	0.946	0.878
	35	0.706	0.700	0.712	0.761	0.823	0.922	1.014	1.098	1.156	1.178	1.156	1.071	1.044	0.978	0.925
	40	0.746	0.728	0.738	0.782	0.864	0.974	1.068	1.176	1.202	1.226	1.192	1.135	1.096	1.024	0.964
$\theta = 90^{\circ}$	0	0.165	0.165	0.165	0.165	0.165	0.163	0.163	0.165	0.165	0.165	0.165	0.165	0.165	0.165	0.165
	1	0.342	0.333	0.321	0.328	0.333	0.341	0.358	0.356	0.347	0.345	0.341	0.341	0.328	0.324	0.316
	2	0.381	0.372	0.372	0.378	0.386	0.398	0.402	0.418	0.432	0.438	0.438	0.416	0.402	0.396	0.384
	4	0.402	0.399	0.402	0.408	0.422	0.431	0.442	0.466	0.481	0.489	0.481	0.460	0.442	0.420	0.402
	6	0.422	0.420	0.429	0.458	0.480	0.506	0.530	0.552	0.572	0.578	0.560	0.537	0.501	0.470	0.442
	8	0.458	0.450	0.461	0.483	0.517	0.542	0.578	0.604	0.625	0.637	0.611	0.588	0.542	0.510	0.478
	10	0.497	0.494	0.503	0.529	0.581	0.602	0.640	0.682	0.717	0.743	0.702	0.673	0.629	0.586	0.524
	15	0.558	0.552	0.578	0.627	0.703	0.737	0.790	0.849	0.918	0.916	0.895	0.852	0 811	0.709	0.642
	20	0.590	0.592	0.613	0.664	0.730	0.802	0.857	0.922	0.994	1.001	0.994	0.942	0.878	0.790	0.709
	25	0.618	0.611	0.637	0.688	0.756	0.822	0.900	0.966	1.038	1.067	1.032	0.990	0.918	0.837	0.762
	30	0.638	0.627	0.642	0.710	0.792	0.880	0.958	1.030	1.078	1.097	1.070	1.022	0.958	0.882	0.792
	35	0.668	0.662	0.683	0.740	0.818	0.907	1.000	1.072	1.128	1.132	1.098	1.046	0.985	0.918	0.850
	40	0.698	0.695	0.718	C.772	0.856	0.941	1.040	1.112	1.157	1.160	1.122	1.071	1.014	0.946	0.887
$\theta = 112\frac{1}{2}^{\circ}$	0	0.165	0.165	0.165	0.163	0.165	0.165	0.165	0.165	0.165	0.167	0.165	0.165	0.165	0.165	0.165
	1	0.307	0.302	0.302	0.309	0.309	0.316	0.322	0.322	0.322	0.318	0.324	0.322	0.309	0.297	0.284
	2	0.343	0.338	0.336	0.342	0.358	0.358	0.375	0.389	0.396	0.403	0.408	0.396	0.381	0.362	0.338
	4	0.343	0.338	0.342	0.354	0.372	0.394	0.398	0.426	0.437	0.442	0.446	0.431	0.412	0.386	0.358
	6	0.356	0.352	0.359	0.376	0.404	0.429	0.457	0.463	0.491	0.498	0.493	0.485	0.456	0.421	0.381
	8	0.372	0.370	0.374	0.388	0.425	0.455	0.502	0.517	0.533	0.546	0.542	0.528	0.498	0.444	0.402
	10	0.399	0.396	0.396	0.409	0.496	0.509	0.548	0.571	0.599	0.628	0.606	0.591	0.574	0.512	0.457
	15	0.418	0.413	0.425	0.466	0.524	0.576	0.624	0.672	0.735	0.775	0.764	0.736	0.680	0.591	0.515
	20	0.446	0.437	0.444	0.484	0.546	0.627	0.675	0.746	0.818	0.852	0.855	0.798	0.732	0.656	0.544
	25	0.452	0.446	0.453	0.492	0.551	0.641	0.726	0.791	0.862	0.900	0.887	0.834	0.756	0.668	0.602
	30	0.464	0.452	0.468	0.500	0.576	0.673	0.765	0.843	0.904	0.932	0.932	0.869	0.798	0.702	0.593
	35	0.473	0.470	0.486	0.508	0.603	0.696	0.774	0.868	0.908	0.932	0.956	0.882	0.815	0.721	0.637
	40	0.480	0.473	0.493	0.514	0.614	0.702	0.796	0.881	0.926	0.946	0.973	0.913	0.842	0.748	0.651

TABLE IV. (Cont) Base Suction Coefficients for 20° jet deflection

θ	C_J \ $\frac{r}{R}$	0.237	0.287	0.337	0.387	0.437	0.487	0.537	0.587	0.637	0.687	0.737	0.787	0.837	0.887	0.937
$\theta = 135^\circ$																
	0	0.165	0.165	0.165	0.165	0.165	0.165	0.167	0.165	0.165	0.163	0.163	0.165	0.165	0.165	0.165
	1	0.277	0.282	0.282	0.286	0.288	0.298	0.304	0.304	0.312	0.302	0.310	0.310	0.298	0.288	0.272
	2	0.317	0.315	0.317	0.320	0.328	0.339	0.345	0.358	0.366	0.381	0.383	0.378	0.363	0.342	0.304
	4	0.298	0.298	0.302	0.308	0.328	0.351	0.368	0.388	0.402	0.402	0.418	0.405	0.388	0.356	0.318
	6	0.298	0.298	0.302	0.308	0.332	0.367	0.390	0.409	0.426	0.438	0.443	0.443	0.421	0.372	0.330
	8	0.290	0.290	0.294	0.302	0.340	0.382	0.420	0.428	0.442	0.469	0.480	0.478	0.456	0.382	0.342
	10	0.290	0.290	0.294	0.302	0.351	0.392	0.436	0.454	0.472	0.508	0.519	0.522	0.490	0.436	0.362
	15	0.290	0.290	0.294	0.302	0.351	0.416	0.468	0.528	0.590	0.638	0.642	0.620	0.562	0.481	0.383
	20	0.290	0.290	0.294	0.302	0.362	0.440	0.517	0.587	0.659	0.700	0.702	0.658	0.591	0.502	0.396
	25	0.290	0.290	0.294	0.302	0.362	0.452	0.542	0.622	0.698	0.746	0.753	0.682	0.607	0.518	0.402
	30	0.290	0.290	0.294	0.302	0.380	0.473	0.565	0.651	0.730	0.785	0.780	0.717	0.636	0.522	0.413
	35	0.290	0.290	0.294	0.302	0.392	0.492	0.584	0.675	0.752	0.810	0.802	0.739	0.655	0.540	0.422
	40	0.290	0.290	0.294	0.302	0.408	0.515	0.605	0.690	0.771	0.832	0.830	0.760	0.670	0.561	0.430
$\theta = 157\frac{1}{2}^\circ$																
	0	0.165	0.165	0.163	0.165	0.165	0.165	0.167	0.167	0.167	0.165	0.165	0.163	0.163	0.165	0.163
	1	0.270	0.266	0.266	0.266	0.280	0.284	0.298	0.298	0.306	0.292	0.298	0.298	0.286	0.278	0.274
	2	0.302	0.296	0.296	0.308	0.324	0.330	0.342	0.350	0.358	0.365	0.369	0.362	0.350	0.336	0.302
	4	0.285	0.280	0.280	0.296	0.309	0.323	0.342	0.361	0.361	0.372	0.385	0.371	0.364	0.336	0.302
	6	0.263	0.257	0.272	0.283	0.302	0.331	0.345	0.367	0.384	0.390	0.402	0.395	0.362	0.328	0.300
	8	0.256	0.248	0.258	0.272	0.302	0.338	0.345	0.376	0.395	0.402	0.416	0.407	0.386	0.343	0.309
	10	0.248	0.244	0.244	0.258	0.308	0.338	0.356	0.382	0.407	0.426	0.420	0.413	0.402	0.374	0.315
	15	0.248	0.242	0.246	0.256	0.304	0.338	0.373	0.413	0.426	0.445	0.466	0.435	0.417	0.381	0.328
	20	0.237	0.237	0.237	0.256	0.306	0.342	0.382	0.431	0.456	0.485	0.502	0.476	0.448	0.413	0.354
	25	0.235	0.232	0.237	0.256	0.310	0.355	0.394	0.456	0.483	0.517	0.523	0.506	0.473	0.437	0.366
	30	0.235	0.232	0.239	0.256	0.314	0.368	0.419	0.478	0.516	0.558	0.564	0.500	0.481	0.458	0.402
	35	0.235	0.236	0.237	0.256	0.325	0.376	0.431	0.492	0.530	0.573	0.587	0.525	0.502	0.461	0.396
	40	0.235	0.232	0.237	0.256	0.331	0.376	0.442	0.506	0.554	0.606	0.618	0.546	0.508	0.478	0.387
$\theta = 180^\circ$																
	0	0.165	0.165	0.165	0.165	0.165	0.167	0.167	0.165	0.165	0.165	0.163	0.163	0.165	0.165	0.165
	1	0.268	0.266	0.264	0.268	0.280	0.286	0.298	0.302	0.302	0.288	0.298	0.298	0.282	0.278	0.274
	2	0.296	0.296	0.302	0.318	0.320	0.326	0.338	0.347	0.358	0.363	0.363	0.361	0.352	0.320	0.291
	4	0.280	0.280	0.286	0.298	0.307	0.320	0.338	0.347	0.358	0.363	0.363	0.361	0.352	0.320	0.291
	6	0.242	0.240	0.244	0.258	0.272	0.296	0.320	0.342	0.360	0.368	0.372	0.368	0.356	0.320	0.291
	8	0.226	0.228	0.234	0.242	0.262	0.288	0.316	0.342	0.360	0.368	0.372	0.368	0.356	0.320	0.291
	10	0.208	0.212	0.220	0.232	0.256	0.288	0.316	0.342	0.364	0.380	0.382	0.378	0.363	0.332	0.298
	15	0.198	0.201	0.216	0.232	0.256	0.288	0.316	0.342	0.368	0.397	0.402	0.397	0.376	0.345	0.302
	20	0.198	0.201	0.216	0.232	0.256	0.288	0.316	0.342	0.368	0.404	0.418	0.410	0.386	0.350	0.308
	25	0.198	0.201	0.216	0.232	0.256	0.288	0.316	0.342	0.368	0.404	0.426	0.418	0.390	0.350	0.308
	30	0.198	0.201	0.216	0.232	0.256	0.288	0.316	0.342	0.368	0.415	0.434	0.420	0.396	0.359	0.312
	35	0.198	0.201	0.216	0.232	0.256	0.288	0.316	0.342	0.368	0.430	0.441	0.423	0.400	0.365	0.320
	40	0.188	0.190	0.200	0.221	0.248	0.272	0.301	0.343	0.388	0.446	0.448	0.427	0.402	0.365	0.320

TABLE V.

Variation of C_p ratio with C_J ratio for the jet in the overchoked state.

C_p ratio $\dfrac{C_p \text{ with jet at overchoked } C_J}{C_p \text{ with jet at choking } C_J}$

C_J ratio $\dfrac{\text{overchoked value of } C_J}{\text{choking value of } C_J}$

$\frac{C_J}{C_J(\text{choking})}$	δ = 0°	δ = 2° θ = 0°	45°	90°	135°	180°	δ = 5° θ = 0°	45°	90°	135°	180°
1.0	1.0	1.0	1.0	1.0	1.0	1.0	1.0	1.0	1.0	1.0	1.0
1.1	0.95	0.95	0.95	0.95	0.96	0.96	0.95	0.96	0.96	0.96	0.96
1.2	0.92	0.92	0.93	0.93	0.94	0.93	0.92	0.92	0.92	0.94	0.94
1.4	0.90	0.90	0.90	0.91	0.91	0.92	0.90	0.91	0.90	0.91	0.91
1.6	0.89	0.90	0.90	0.90	0.90	0.91	0.90	0.90	0.91	0.91	0.92
1.8	0.89	0.90	0.89	0.90	0.91	0.91	0.90	0.90	0.91	0.91	0.90
		δ = 10° θ = 0°	45°	90°	135°	180°	δ = 20° θ = 0°	45°	90°	135°	180°
1.0		1.0	1.0	1.0	1.0	1.0	1.0	1.0	1.0	1.0	1.0
1.1		.97	.96	.97	.98	.98	.97	.96	.98	.98	.98
1.2		.94	.94	.94	.95	.96	.95	.95	.96	.97	.97
1.4		.92	.94	.94	.94	.94	.92	.94	.94	.95	.95
1.6		.92	.94	.92	.92	.92	.92	.92	.93	.94	.94
1.8		.91	.91	.91	.91	.91	.92	.92	.92	.94	.94